

## Article

# The Solar Particle Acceleration Radiation and Kinetics (SPARK) Mission Concept

Hamish A. S. Reid <sup>1,\*</sup>, Sophie Musset <sup>2</sup>, Daniel F. Ryan <sup>3</sup>, Vincenzo Andretta <sup>4</sup>, Frédéric Auchère <sup>5</sup>, Deborah Baker <sup>1</sup>, Federico Benvenuto <sup>6</sup>, Philippa Browning <sup>7</sup>, Éric Buchlin <sup>5</sup>, Ariadna Calcines Rosario <sup>8</sup>, Steven D. Christe <sup>9</sup>, Alain Jody Corso <sup>10</sup>, Joel Dahlin <sup>11</sup>, Silvia Dalla <sup>12</sup>, Giulio Del Zanna <sup>13</sup>, Carsten Denker <sup>14</sup>, Jaroslav Dudík <sup>15</sup>, Robertus Erdélyi <sup>16,17,18</sup>, Iaria Ermolli <sup>19</sup>, Lyndsay Fletcher <sup>20,21</sup>, Andrzej Fludra <sup>22</sup>, Lucie M. Green <sup>1</sup>, Mykola Gordovskyy <sup>23</sup>, Salvo L. Guglielmino <sup>19</sup>, Iain Hannah <sup>20</sup>, Richard Harrison <sup>22</sup>, Laura A. Hayes <sup>2</sup>, Andrew R. Inglis <sup>9,24</sup>, Natasha L. S. Jeffrey <sup>25</sup>, Jana Kašparová <sup>15</sup>, Graham S. Kerr <sup>9,24</sup>, Christian Kintziger <sup>26</sup>, Eduard P. Kontar <sup>20</sup>, Säm Krucker <sup>3,27</sup>, Timo Laitinen <sup>12</sup>, Philippe Laurent <sup>28</sup>, Olivier Limousin <sup>28</sup>, David M. Long <sup>29</sup>, Shane A. Maloney <sup>30</sup>, Paolo Massa <sup>31</sup>, Anna Maria Massone <sup>6</sup>, Sarah Matthews <sup>1</sup>, Tomasz Mrozek <sup>32</sup>, Valery M. Nakariakov <sup>33</sup>, Susanna Parenti <sup>5</sup>, Michele Piana <sup>6,34</sup>, Vanessa Polito <sup>35,36</sup>, Melissa Pesce-Rollins <sup>37</sup>, Paolo Romano <sup>19</sup>, Alexis P. Rouillard <sup>38</sup>, Clementina Sasso <sup>4</sup>, Albert Y. Shih <sup>9</sup>, Marek Stęślicki <sup>31</sup>, David Orozco Suárez <sup>39,40</sup>, Luca Teriaca <sup>41</sup>, Meetu Verma <sup>13</sup>, Astrid M. Veronig <sup>42</sup>, Nicole Vilmer <sup>43</sup>, Christian Vocks <sup>13</sup>, and Alexander Warmuth <sup>13</sup>

<sup>1</sup> Mullard Space Science Laboratory, University College London, Holmbury Hill Rd, Dorking RH5 6NT, UK; sarah.matthews@ucl.ac.uk

<sup>2</sup> European Space Research and Technology Centre, 2201 Noordwijk, The Netherlands

<sup>3</sup> FHNW Institute for Data Science, University of Applied Sciences and Arts Northwestern Switzerland, Bahnhofstrasse 6, 5210 Windisch, Switzerland

<sup>4</sup> INAF/Capodimonte Astronomical Observatory, 80131 Naples, Italy; vincenzo.andretta@inaf.it

<sup>5</sup> CNRS, Institut d'Astrophysique Spatiale, Université Paris-Saclay, 91405 Orsay, France; susanna.parenti@universite-paris-saclay.fr

<sup>6</sup> MIDA, Dipartimento di Matematica, Università di Genova, 16146 Genova, Italy; massone@dima.unige.it (A.M.M.); piana@dima.unige.it (M.P.)

<sup>7</sup> Jodrell Bank Centre for Astrophysics, University of Manchester, Manchester M13 9PL, UK; philippa.browning@manchester.ac.uk

<sup>8</sup> Centre for Advanced Instrumentation, Durham University, Durham DH1 3LE, UK

<sup>9</sup> NASA Goddard Space Flight Center, Heliophysics Science Division, Code 671, Greenbelt, MD 20771, USA; kerrg@cua.edu (G.S.K.); albert.y.shih@nasa.gov (A.Y.S.)

<sup>10</sup> National Research Council of Italy, Institute for Photonics and Nanotechnologies, Via Trasea 7, 35131 Padova, Italy; alain.corso@pd.ifi.cnr.it

<sup>11</sup> Astronomy Department, University of Maryland, College Park, MD 20740, USA

<sup>12</sup> Jeremiah Horrocks Institute, University of Central Lancashire, Preston PR1 2HE, UK

<sup>13</sup> DAMTP, Centre for Mathematical Sciences, University of Cambridge, Wilberforce Road, Cambridge CB3 0WA, UK; g.del-zanna@damtp.cam.ac.uk (G.D.Z.); cvocks@aip.de (C.V.); awarmuth@aip.de (A.W.)

<sup>14</sup> Leibniz-Institut für Astrophysik Potsdam (AIP), An der Sternwarte 16, 14482 Potsdam, Germany

<sup>15</sup> Astronomical Institute of the Czech Academy of Sciences, Fričova 298, 251 65 Ondřejov, Czech Republic; jana.kasparova@asu.cas.cz

<sup>16</sup> Solar Physics & Space Plasma Research Center (SP2RC), School of Mathematics and Statistics, University of Sheffield, Hounsfield Road, Sheffield S3 7RH, UK; robertus@sheffield.ac.uk

<sup>17</sup> Department of Astronomy, Eötvös Loránd University, Pázmány Péter sétány 1/A, H-1117 Budapest, Hungary

<sup>18</sup> Gyula Bay Zoltan Solar Observatory (GSO), Hungarian Solar Physics Foundation (HSPF), Petőfi tér 3., H-5700 Gyula, Hungary

<sup>19</sup> INAF—Catania Astrophysical Observatory, 95123 Catania, Italy; ilaria.ermolli@inaf.it (I.E.); salvatore.guglielmino@inaf.it (S.L.G.)

<sup>20</sup> School of Physics and Astronomy, University of Glasgow, Glasgow G12 8QQ, UK;

lyndsay.fletcher@glasgow.ac.uk (L.F.); iain.hannah@glasgow.ac.uk (I.H.)

<sup>21</sup> Rosseland Centre for Solar Physics, University of Oslo, P.O. Box 1029 Blindern, NO-0315 Oslo, Norway

<sup>22</sup> RAL Space, STFC Rutherford Appleton Laboratory, Chilton, Didcot OX11 0QX, UK;

andrzej.fludra@stfc.ac.uk (A.F.); richard.harrison@stfc.ac.uk (R.H.)

<sup>23</sup> Department of Physics, Astronomy and Mathematics, University of Hertfordshire, Hatfield AL10 9AB, UK

<sup>24</sup> Department of Physics, Catholic University of America, Washington, DC 20064, USA

<sup>25</sup> Department of Mathematics, Physics & Electrical Engineering, Northumbria University, Newcastle upon Tyne NE1 8ST, UK



**Citation:** Reid, H.A.S.; Musset, S.; Ryan, D.F.; Andretta, V.; Auchère, F.; Baker, D.; Benvenuto, F.; Browning, P.; Buchlin, É.; Calcines Rosario, A.; et al. The Solar Particle Acceleration Radiation and Kinetics (SPARK) Mission Concept. *Aerospace* **2023**, *10*, 1034. <https://doi.org/10.3390/aerospace10121034>

Academic Editor: Paolo Tortora

Received: 31 October 2023

Revised: 1 December 2023

Accepted: 5 December 2023

Published: 15 December 2023



**Copyright:** © 2023 by the authors. Licensee MDPI, Basel, Switzerland. This article is an open access article distributed under the terms and conditions of the Creative Commons Attribution (CC BY) license (<https://creativecommons.org/licenses/by/4.0/>).

- <sup>26</sup> Centre Spatial de Liège, University of Liège (ULiège)—STAR Institute, 4000 Liège, Belgium; ckintziger@uliege.be
- <sup>27</sup> Space Sciences Lab, UC Berkeley, 7 Gauss Way, Berkeley, CA 94708, USA
- <sup>28</sup> Université Paris-Saclay, Université Paris Cité, CEA, CNRS, AIM, 75205 Paris, France; philippe.laurent@cea.fr (P.L.); olivier.limousin@cea.fr (O.L.)
- <sup>29</sup> Astrophysics Research Centre, School of Mathematics and Physics, Queen’s University Belfast, University Road, Belfast BT7 1NN, UK
- <sup>30</sup> Dublin Institute of Advanced Studies, 31 Fitzwilliam Place, D02 XF86 Dublin, Ireland; shane.maloney@dias.ie
- <sup>31</sup> Department of Physics & Astronomy, Western Kentucky University, Bowling Green, KY 42101, USA
- <sup>32</sup> Centrum Badań Kosmicznych PAN, Bartycka 18A, 00-716 Warszawa, Poland; tmrozek@cbk.pan.wroc.pl
- <sup>33</sup> Physics Department, University of Warwick, Coventry CV4 7AL, UK
- <sup>34</sup> Osservatorio Astrofisico di Torino, Istituto Nazionale di Astrofisica, 10025 Pino Torinese, Italy
- <sup>35</sup> Lockheed Martin Solar and Astrophysics Laboratory, Building 252, 3251 Hanover Street, Palo Alto, CA 94304, USA
- <sup>36</sup> Department of Physics, Oregon State University, Corvallis, OR 97331, USA
- <sup>37</sup> Istituto Nazionale di Fisica Nucleare, Sezione di Pisa, 56127 Pisa, Italy
- <sup>38</sup> IRAP, Université Toulouse III—Paul Sabatier, CNRS, CNES, 31062 Toulouse, France
- <sup>39</sup> Instituto de Astrofísica de Andalucía (IAA-CSIC), 18008 Granada, Spain; orozco@iaa.es
- <sup>40</sup> Spanish Space Solar Physics Consortium (S<sup>3</sup>PC), 18008 Granada, Spain
- <sup>41</sup> Max Planck Institute for Solar System Research, 37077 Göttingen, Germany
- <sup>42</sup> Institute of Physics & Kanzelhöhe Observatory for Solar and Environmental Research, University of Graz, 8010 Graz, Austria
- <sup>43</sup> LESIA, Observatoire de Paris, Université PSL, CNRS, Sorbonne Université, Université Paris Cité, 5 place Jules Janssen, 92195 Meudon, France; nicole.vilmer@obspm.fr
- \* Correspondence: hamish.reid@ucl.ac.uk

**Abstract:** Particle acceleration is a fundamental process arising in many astrophysical objects, including active galactic nuclei, black holes, neutron stars, gamma-ray bursts, accretion disks, solar and stellar coronae, and planetary magnetospheres. Its ubiquity means energetic particles permeate the Universe and influence the conditions for the emergence and continuation of life. In our solar system, the Sun is the most energetic particle accelerator, and its proximity makes it a unique laboratory in which to explore astrophysical particle acceleration. However, despite its importance, the physics underlying solar particle acceleration remain poorly understood. The SPARK mission will reveal new discoveries about particle acceleration through a uniquely powerful and complete combination of  $\gamma$ -ray, X-ray, and EUV imaging and spectroscopy at high spectral, spatial, and temporal resolutions. SPARK’s instruments will provide a step change in observational capability, enabling fundamental breakthroughs in our understanding of solar particle acceleration and the phenomena associated with it, such as the evolution of solar eruptive events. By providing essential diagnostics of the processes that drive the onset and evolution of solar flares and coronal mass ejections, SPARK will elucidate the underlying physics of space weather events that can damage satellites and power grids, disrupt telecommunications and GPS navigation, and endanger astronauts in space. The prediction of such events and the mitigation of their potential impacts are crucial in protecting our terrestrial and space-based infrastructure.

**Keywords:** particle acceleration; magnetic reconnection; instrumentation; corona; coronal mass ejections (CMEs); flares; extreme ultraviolet; X-rays; gamma rays

## 1. Scientific Objectives

The SPARK mission concept aims to investigate solar particle acceleration and the magnetic energy release that powers it by observing solar eruptive events, the most energetic and geo-effective drivers of space weather.

In the standard model of solar eruptive events (Figure 1; see also [1]), highly stressed magnetic fields reconnect in the low corona, thereby impulsively releasing vast amounts of energy. Depending on the magnetic configuration, plasma, magnetic field, and accelerated

particles may escape into the heliosphere as coronal mass ejections (CMEs), “jets”, or solar energetic particles (SEPs), which directly contribute to space weather. Accelerated particles also spiral downward around magnetic field lines (“loops”) towards the chromospheric “footpoints”, depositing their energy as they propagate. This heats and ionises the plasma in the chromosphere, transition region (TR), and lower corona, producing the intense broadband radiation known as a solar flare. The rapid heating creates a high-pressure region that ablates material back up along the loops in a process known as chromospheric “evaporation”, which causes the loops to radiate in extreme ultraviolet (EUV) and soft X-rays. Additionally, plasma in and above the loops can be directly heated by the energy release and/or acceleration process.

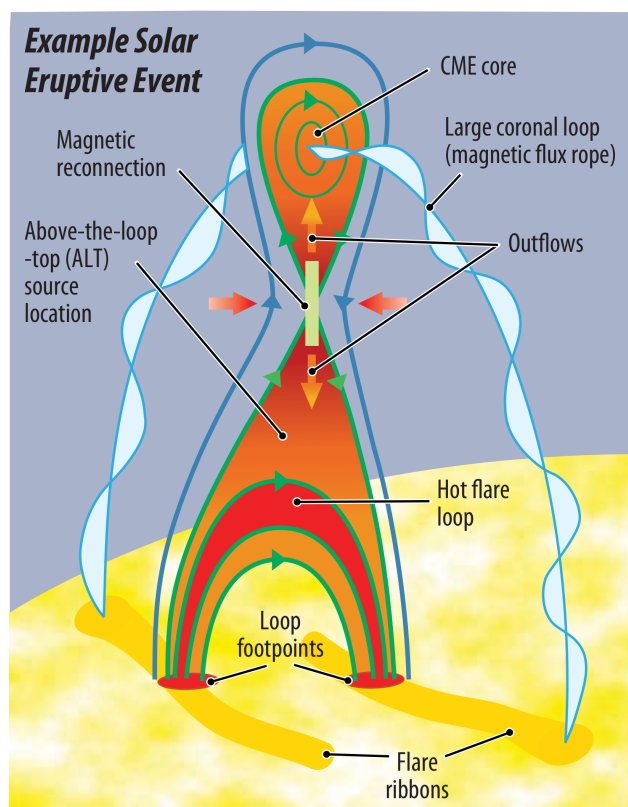


**Figure 1.** SPARK captures all elements of a solar eruptive event (the combination of a flare and a CME) identified in this cartoon. FOXSI images the HXR signatures of accelerated electrons and hot plasma at all locations. LISSAN captures the  $\gamma$ -ray signatures of accelerated ions and the most energetic electrons, and SISA reveals the lower atmospheric response and EUV structure in the corona. Figure courtesy of the FIERCE proposal team and the FOXSI SMEX proposal team.

The particles in solar eruptive events can be divided into three populations: hot plasmas, accelerated electrons, and accelerated ions. One of the most useful diagnostics for characterising thermalised and accelerated electrons is the X-ray bremsstrahlung emission they produce as they scatter in the ambient medium. The bremsstrahlung spectrum reflects the velocity distribution of the particles that produced it and can be inverted to reconstruct the spectrum of the emitting electrons [2,3]. This means hot plasma and accelerated electrons can be distinguished by their Maxwellian (thermal) and power-law (non-thermal) shaped spectra, e.g., [4–6]. Thermal emission tends to dominate in the soft X-ray (SXR; typically below 20 keV) regime, while non-thermal emission tends to dominate in the hard X-ray (HXR; typically higher than 20 keV) regime. X-rays can provide straightforward measurements of the numbers and energies of accelerated electrons not available from other wavelengths or requiring non-trivial assumptions when observed in microwaves. Hence, X-rays can provide a deeper understanding of the underlying acceleration process.

Accelerated ions are even less well understood than electrons due to the difficulties encountered in observing their  $\gamma$ -ray emission. Accelerated ions in the range of 1–100 MeV/nucleon can be detected via various  $\gamma$ -ray lines in the range of 1–10 MeV due to nuclear de-excitation, neutron capture, and positron annihilation [7–14]. Accelerated ions with energies greater than 100 MeV/nucleon can be detected via the decay of secondary pions via nuclear reactions with the ambient medium. As the pions decay, the decay products produce a broadband continuum at photon energies above 10 MeV, with a broad peak around 70 MeV from neutral pion radiation [15,16].

Although the principal points of the standard model are established, many questions remain regarding the fundamental processes of particle acceleration, impulsive energy release, and energy transport. However, the key scientific measurements required to answer these questions have not been possible with previous instruments. Solar  $\gamma$ -ray line emission has been imaged in one flare [17] and only localised through centroids in an additional four [14]. Consequently, the spatiotemporal evolution of accelerated ions has never been revealed. The role of ion acceleration in solar eruptive events therefore remains largely unknown, despite evidence that ions accelerated in flares may carry an energy comparable to that of accelerated electrons, e.g., [18–20]. Previous HXR spectroscopic imaging observations (e.g., RHESSI [21] and Solar Orbiter/STIX [22]) have not provided sufficient sensitivity to reliably observe accelerated electrons and direct plasma heating in the corona, where the acceleration is believed to take place. This is because the intensity of bremsstrahlung depends on the ambient density, which is typically very low in the corona, preventing observational tests of different acceleration models. Additionally, previous instruments have not provided a sufficient dynamic range ( $\geq 100$ ) to simultaneously observe the emission from the corona and the chromosphere, where the density (and, hence, emission), is much greater. This has limited our understanding of how transport effects alter the distribution of accelerated particles. Moreover, past and current X-ray images like RHESSI and STIX are limited by the use of an indirect Fourier imaging technique, which causes source areas and shapes to be only approximate. Additionally, imaging on second and subsecond time scales relevant to particle acceleration has not yet been achieved. Finally, current EUV imaging spectrographs (e.g., Hinode/EIS [23] and Solar Orbiter/SPICE [24]) have provided intriguing images of the complex structures associated with solar eruptive events, but they have not been optimised for solar eruptive events. Their typical single-slit design and operational priorities have led EUV spectra to rarely be available on the right timescales, at the right times, and in the right locations to compare with X-ray and  $\gamma$ -ray observations. The Solar-C Extreme-UV High-throughput Solar Telescope (EUVST; [25]) and the Multi-Slit Solar Explorer (MUSE; [26–28]) are highly complementary upcoming EUV missions that will be transformative for flare science [28]. MUSE will provide high-cadence active region-scale imaging spectroscopy, sampling select key EUV lines by rastering its 35 slits. EUVST, with its single slit, will provide much broader temperature coverage, with rich plasma diagnostics from a large number of lines. Both instruments are scheduled to launch within one year of each other and promise cospatial observations of plasma in the solar atmosphere. An instrument that would build upon their science legacy—one that co-observes with X-ray and  $\gamma$ -ray instruments—should be the aim of a next-generation flare mission, that is, an instrument that combines rich plasma diagnostics with very high-cadence 2D spectral imaging.

SPARK will overcome all these challenges with its unique combination of high-sensitivity, fast spectroscopic imaging in  $\gamma$ -ray, X-ray, and EUV, optimised for solar eruptive events. It will address four specific fundamental science questions:

1. How does impulsive energy release accelerate particles in the solar atmosphere?
2. How is impulsively released energy transported and dissipated in the solar atmosphere?
3. What are the physical low-corona origins of space weather events?
4. How is the corona above active regions heated?

By addressing these questions, SPARK will elucidate fundamental physical processes that are ubiquitous throughout our Universe and drive space weather events that have direct consequences for our technologies and way of life.

### 1.1. How Does Impulsive Energy Release Accelerate Particles in the Solar Atmosphere?

Accelerated charged particles constitute a significant fraction (up to tens of percent) of the magnetic energy released in the most energetic space weather events, e.g., [19,29]. Observationally distinguishing between acceleration models requires the number, location, and evolution of multiple faint thermal and non-thermal sources near the coronal acceleration region to be characterized in the presence of much more intense chromospheric footpoint emission. SPARK's unique combination of high dynamic range and high-sensitivity imaging spectroscopy in the  $\gamma$ -ray, X-ray, and EUV regimes at timescales relevant to the underlying physical processes will make this possible for the first time.

#### 1.1.1. Where and When Do Particle Acceleration and Local Plasma Heating Occur?

The two most likely models to explain the high acceleration efficiency of electrons are the Fermi acceleration process through the evolution and merging of "magnetic islands" [30,31] created by the reconnection, as well as a second-order Fermi acceleration process in the turbulent plasma of the reconnection outflow jets with or without termination shocks [32–35]. The magnetic-island model predicts that both electron acceleration and direct plasma heating occur near the reconnection site(s) in the current sheet and that direct plasma heating precedes electron acceleration [30]. Conversely, the stochastic model predicts that acceleration and direct heating occur simultaneously but significantly separated from the reconnection site in both upward and downward outflow jets (see Figure 2). Concerning ion acceleration, a detailed study of individual large events showed differences between ion and electron time evolution during the course of a flare [36]. The one flare imaged in the  $\gamma$ -ray line with RHESSI and the four for which emission centroid locations were calculated showed significant displacements between HXR and  $\gamma$ -ray line sources, indicating spatial displacements between electron and ion energy release sites [14,17]. SPARK will reveal, for the first time, where electron acceleration and direct heating occur with respect to the reconnection site, as well as under what scenarios the different acceleration models dominate, and reveal the relationship between electron and ion acceleration. This will be achieved with subsecond X-ray spectral imaging with sufficient spatial resolution to separate the various sources. SPARK will compare  $\gamma$ -ray and X-ray signatures of energetic electrons and ions in combination with the EUV non-Gaussian line profiles that are a signature of non-Maxwellian ion velocity distributions. Using increased X-ray sensitivity and dynamic range, SPARK will characterize the spectrum of the accelerated electrons in the corona, even in the presence of much brighter chromospheric emission. SPARK will provide complementary measurements of the coronal magnetic field from Fe X lines emitted around 1 MK. In addition, it will chart the plasma response to heating via the hot Fe XXIII and Fe XXIV (15–20 MK) spectral lines and determine the relative plasma abundances to differentiate between coronal and ablated chromospheric plasma.

#### 1.1.2. What Are the Efficiency and Energy Content of Electron and Ion Acceleration?

The fraction of particles accelerated out of the ambient Maxwellian velocity distribution and the total energy they contain are essential constraints on acceleration models. Acceleration by magnetic islands [30] and super-Dreicer electric fields in a reconnecting current sheet [37] can accelerate a large fraction of the available electrons, while mechanisms relying on large-scale sub-Dreicer electric fields cannot [38]. SPARK will determine the number and energy of accelerated particles with an accuracy not previously possible. With a significantly enhanced X-ray dynamic range, SPARK will measure the non-thermal spectra of coronal and footpoint sources down to lower energies whilst constraining the relative number of accelerated particles of different ion species (e.g., alpha/proton ratio [36]).

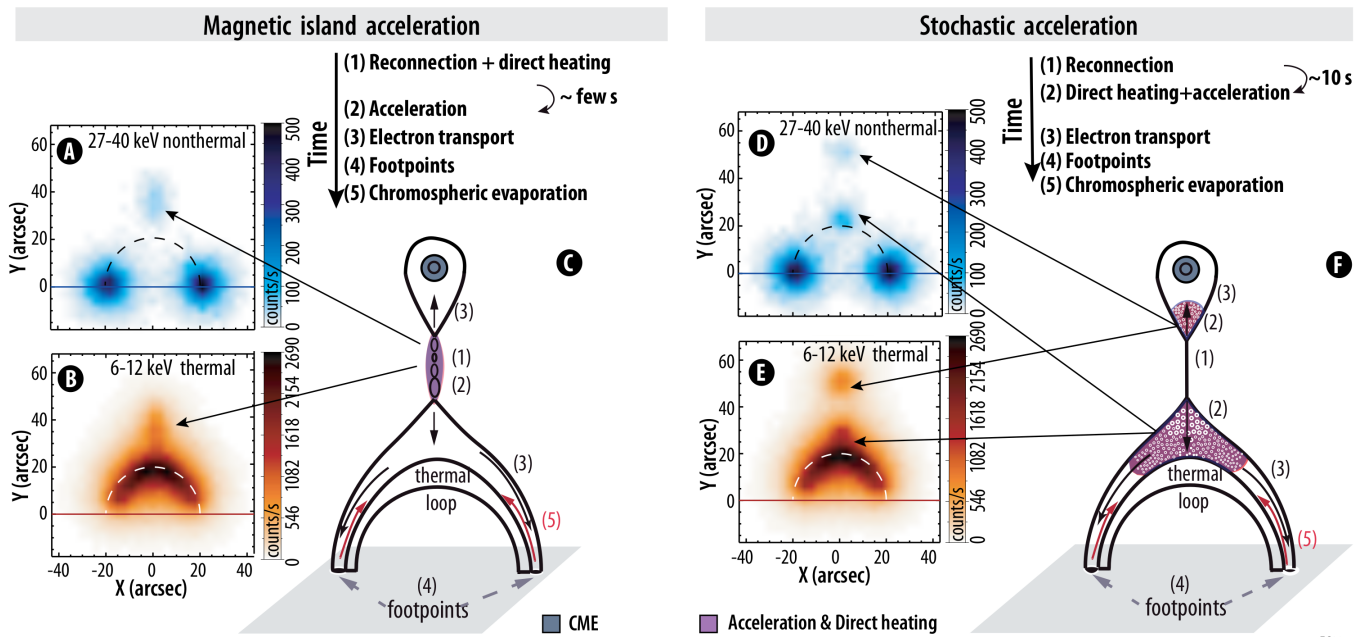


**Figure 2.** SPARK will distinguish between different models of flare particle acceleration. In these 2D flare cartoons, the locations and chronological order of various X-ray- and EUV-producing processes differ between the two most likely models of electron acceleration in eruptive flares: magnetic island-merging acceleration (**left**) and stochastic (second-order Fermi) acceleration (**right**). Simulated FOXSI detector response images of non-thermal electrons (blue) and thermal plasma (orange) are shown as insets. Figure courtesy of the FIERCE proposal team.

### 1.1.3. How Do Electron and Ion Acceleration and Transport Differ in the Flaring Atmosphere?

Theoretical studies show that differences between the acceleration and transport of electrons and ions can be used as a unique diagnostic tool for the processes in the magnetic reconnection region, as well as the geometry of the magnetic field in and around it. The lack of spatially resolved  $\gamma$ -ray observations of accelerated ions is therefore a significant obstacle to constructing a comprehensive solar flare model. With significantly upgraded spatial resolution in the  $\gamma$ -ray regime, SPARK will enable major advances in our understanding of how ions are accelerated and transported in flares and how their dynamics differ from the dynamics of energetic electrons and in using energetic ions as an important diagnostic tool for non-thermal plasma in the flaring corona.

### 1.1.4. Where and How Are the Most Energetic Particles Accelerated at the Sun?

Studies of small numbers of events examining  $\gamma$ -ray lines (1–10 MeV) and the pion continuum ( $>10$  MeV) suggest that the accelerated ion spectrum is not a simple power law extending from non-relativistic (1–100 MeV/nucleon) to relativistic ( $>$  few hundred MeV/nucleon) regimes, e.g., [39–43]. This raises the question of whether the most energetic particles are accelerated via a different mechanism to those at lower energies. The longevity of some pion emission presents another major challenge to our understanding of how the most energetic solar particles are accelerated, e.g., [44,45]. The high-sensitivity HXR and  $\gamma$ -ray spectroscopy of SPARK will facilitate a comprehensive study of the timing and spectra of electron bremsstrahlung and pion decay radiation in a significant number of events for the first time. Such observations are essential to unravel the relative roles of flare and interplanetary processes in the acceleration of high-energy ions, especially in long-duration events.

### 1.2. How Is Impulsively Released Energy Transported and Dissipated in the Solar Atmosphere?

SPARK will probe energy-transport processes that link impulsively released magnetic energy to the resultant emission from the lower atmosphere, where the bulk of the flare energy is radiated. This will be done in two ways: by measuring hitherto poorly constrained observational inputs to the latest state-of-the-art numerical models of solar flares, e.g., [46–63] and by providing previously unachievable observations against which the model predictions will be critically interrogated. Such model inputs provided by SPARK include the non-thermal electron and ion energy distributions injected towards the lower solar atmosphere, the ribbon/footpoint source areas, and the preflare atmospheric state (e.g., coronal temperature, density, loop length, and coronal magnetic field).

#### 1.2.1. How and Where Do Accelerated Particles Lose Their Energy in the Corona and Chromosphere?

As flare-accelerated particles exit the coronal acceleration region and propagate along loops, they lose energy through Coulomb collisions with ambient particles, wave–particle interactions, and the generation of return currents [4]. The evolution of the particle distribution as the particles propagate along flare loops depends on (and thus reveals) the relative importance of these mechanisms. The statistically significant separation between HXR and  $\gamma$ -ray line sources in the single resolved RHESSI  $\gamma$ -ray flare image and two of the four RHESSI centroid-localised  $\gamma$ -ray line flares [14,64] may be due to differing acceleration mechanisms. But it may also be due to different transport effects acting on the ions and electrons. We have sparse observations from EUV imaging spectrometers of the kernels of chromospheric evaporation, showing large non-thermal broadenings and upflows in the hotter lines during the impulsive phase (see, e.g., [65–67]), but a clear picture is missing. SPARK will simultaneously observe electrons throughout the flaring structure, image ion emission, and observe the spectral line response of flaring plasma at multiple temperatures. Combining X-rays and EUV imaging spectroscopy, SPARK will facilitate accurate determination of the low-energy part of the electron spectrum, as well as quantifying return current losses. SPARK will, for the first time, constrain accelerated ions transported to the chromosphere using  $\gamma$ rays and the hottest EUV flare lines, like Fe XXIV. Moreover, the combination of X-rays and the multitemperature response of spectral lines will also provide constraints on turbulence present in the solar atmosphere [68].

#### 1.2.2. What Are the Origins of Modulations in Solar Flare Emission?

A key observational feature in flare-associated X-ray emission is the presence of pronounced pulsations and fast-time variations. These modulations, which also appear in many stellar flares, have been observed in thermal and non-thermal emissions across all wavelength regimes, from radio to gamma rays, with characteristic time scales ranging from 0.5 to tens of seconds, e.g., [69–71]. Often, these modulations appear as regular or non-stationary oscillatory patterns, known as “quasi-periodic pulsations”, e.g., [72,73]. However, despite extensive research, the origins of these short-timescale modulations in flare emissions remain debated. While some studies suggest they may be a direct signature of a repetitive impulsive energy-release process, the potential role of magnetohydrodynamic (MHD) oscillations in the flaring site or nearby, particularly in the context of longer-period pulsations, has yet to be fully determined. Similarly, a combination of these processes could be at play (see [71] for an overview of proposed mechanisms). Moreover, it is quite likely that different classes of flaring pulsations (i.e., different periods, patterns, or energies) are produced by different mechanisms. X-ray dynamic-range limitations have not yet allowed us to identify time-varying signatures from different parts of the loop, including the loop-top source. EUV imaging observations have also hindered our ability to locate the modulating emission source due to both cadence constraints and pixel saturation and bleeding during flare events. SPARK enables, for the first time, a full examination of the temporal, spatial, and spectral properties of these pulsations and their relationships across wavelengths, which are essential to determine the origins of the emission modulation.

SPARK will allow us to identify the pulsations in both the thermal and non-thermal regimes in all parts of the flaring loop. Moreover, SPARK will identify whether accelerated protons have similarly associated time variability.

### 1.2.3. What Is the Importance of Accelerated Particles in Transporting Energy Compared with That of Other Mechanisms?

High-frequency Alfvén waves have been proposed as a means of transporting energy from a flare's magnetic reconnection site to the lower atmosphere and heating it, e.g., [74–76]. In recent years, modelling has shown that this is possible [52,60,61]. However, while Alfvén waves are undoubtedly produced during the large-scale reconfiguration of the magnetic field during flares, it is not yet known whether they play a significant role relative to accelerated particles in transporting flare energy and heating flare plasma nor whether other kinds of MHD waves, such as kink and sausage modes, contribute significantly. SPARK will, for the first time, reveal the importance of MHD waves relative to accelerated particles in transporting and dissipating energy in solar eruptive events. SPARK will examine the coronal magnetic field strength and the broadening of certain spectral lines from ions in the EUV passbands formed at different temperatures (see Section 2.3. SPARK will therefore constrain the Poynting flux as the waves propagate and dissipate their energy (see discussions in, e.g., [28]). SPARK will use variations of the chemical composition and elemental abundances to assess the role of MHD waves in transferring energy from the corona into flare kernels (cf. [77] and references therein).

### 1.3. What Are the Physical Low-Corona Origins of Space Weather Events?

An ESA-funded study estimated that the economic cost of a severe space weather event could be as high as EUR 15 billion ([https://esamultimedia.esa.int/docs/business\\_with\\_esa/Space\\_Weather\\_Cost\\_Benefit\\_Analysis\\_ESA\\_2016.pdf](https://esamultimedia.esa.int/docs/business_with_esa/Space_Weather_Cost_Benefit_Analysis_ESA_2016.pdf), accessed on 30 October 2023). This led to the establishment of national forecasting centres across Europe and space weather as a major theme in the ESA's Space Safety programme. Despite this, many questions remain regarding the origins of space weather in the low corona, which act as an impediment to the development of timely and reliable space weather forecasts. SPARK will greatly improve our understanding of the underlying physical processes that drive these events in the low corona and inform the development of future space weather models that aim to deliver timely and accurate forecasts of flares, energetic particles, and eruptions. Knowing about the acceleration process will feed into our understanding of how active regions reach a state whereby a flare or CME is generated. Understanding of the flare initiation process will enable an improved view of the likelihood of a flare occurring in a location that is well placed to impact Earth.

#### 1.3.1. What Are the Energy Content and Spectrum of Sun-Escaping Electrons?

Sun-escaping electrons, components of SEP space weather events, have long been studied in situ at 1 AU [78] and, more recently, closer to the Sun, e.g., [79,80]. However, such observations alone cannot be used to characterise how the electrons are accelerated because the electron distribution is modified by transport effects between the Sun and the observatory. SEP electrons can be observed remotely at the Sun as type III radio bursts (e.g., [81,82]). However, while bulk electron speeds can be inferred from the radio observations, unlike X-rays, they cannot be directly inverted to retrieve the number or energies of accelerated electrons. Therefore, the spectra and acceleration mechanism(s) of solar radio-emitting electrons remain unknown. How these accelerated electrons escape from the flare site is similarly unknown. CMEs and jets offer clear open magnetic paths for particles to escape, but confined flares do not, although interchange reconnection can play a role [83]. Ground-based observations above 10 MHz can be used to image type IIIs [84] but may suffer from intrinsically limited spatial resolution, especially at low frequencies, on account of the radio waves scattering off density inhomogeneities between the source and observer [85,86]. SPARK will provide hitherto unachievable imaging and spectral

observations of accelerated electrons as they escape the Sun [87], facilitated by unprecedented sensitivity and imaging dynamic range in the HXR regime. Such measurements will elucidate the origins of escaping electrons and how they are modified as they propagate towards Earth. SPARK will also test theories of the origins of the slow solar wind by detecting the locations in active region peripheries where particles are accelerated and escape via HXR emissions and upward flows detected in EUV-emitting plasma.

### 1.3.2. What Are the Dominant Initiation Mechanisms of Solar Eruptions?

Many models of the initiation of solar eruptive events involve magnetic reconnection, which results in plasma heating [88,89] and particle acceleration [90]. However, different models of CME initiation predict observationally differentiable locations of the erupting flux rope in relation to where the reconnection starts and, consequently, for the associated X-ray and EUV emissions. The internal tether-cutting model [91,92] predicts that reconnection occurs below the flux rope before the fast takeoff of the eruption. The breakout model [93] predicts that the reconnection occurs above the flux rope before fast takeoff, and the ideal MHD instability model [94] predicts that the flux rope begins to rise before reconnection occurs in either place. It is unclear if the same mechanisms driving the large-scale CMEs are also at play in these smaller events. Some models of jets involve breakout reconnection, e.g., [95], similar to the breakout model for CMEs, while others involve interchange magnetic reconnection [96–98]. SPARK will produce observations of the faint X-ray and EUV emissions linked to particle acceleration and plasma heating during the formation and initiation of solar eruptions for the first time. This will enable discrimination between the many physical processes proposed for the creation of the conditions necessary for an eruption. SPARK will also provide measurements of the plasma dynamics and of the magnetic field of the active region and filament before and during the eruption. Hence, SPARK will provide constraints on the configuration and evolution of the magnetic structure leading to solar eruptions.

### 1.4. How Is the Corona Above Active Regions Heated?

A long-standing enigma in solar and stellar physics is how a star's atmosphere can be orders of magnitude hotter than its surface. This temperature difference requires some form of non-radiative heating, but whether the dominant mechanism is the dissipation of Alfvén waves or impulsive heating by nanoflares has not been established [99–103]. SPARK will enable breakthroughs with respect to this fundamental problem using two approaches. First, SPARK will determine if the characteristics of energy release in the smallest detectable events are fundamentally different from those in larger flares. Secondly, SPARK will statistically determine ensemble properties of heating events too small to be detected individually.

#### 1.4.1. Is Particle Acceleration Ubiquitous among Energy-Release Events at All Size Scales?

The number of flares as a function of their thermal energy follows a power law over several orders of magnitude [104]. This suggests that the underlying energy-release process scales similarly. If nanoflares are part of this distribution, they, too, would be expected to accelerate electrons. Indirect evidence from UV transients suggests that accelerated electrons are indeed present [105,106]. RHESSI and STIX observations have shown that in microflares, the X-ray spectral index is steeper than in larger flares [107–113], suggesting that they are less efficient at accelerating electrons. This was confirmed in a few observations of fainter microflares with NuSTAR during its limited solar campaigns [114–117]. Additional support comes from studies of the thermal–non-thermal energy partition (cf. [118]), which shows that in weaker flares there may not be a sufficient amount of energetic electrons to heat the thermal plasma. SPARK will determine how the energy-release process scales across eight orders of magnitude in energy, from the largest flares ( $\sim 10^{33}$  ergs) down to flares at  $10^{25}$  ergs (2 orders of magnitude smaller than those observed by RHESSI and STIX). SPARK will observe hundreds of thousands of flares below GOES C class and will

provide a comprehensive investigation of events two orders of magnitude less energetic than ever before.

#### 1.4.2. How Does Small-Scale Particle Acceleration Contribute to Coronal Heating?

The presence of temperatures exceeding 5 MK in the non-flaring active regions would provide strong evidence of impulsive, low-frequency nanoflare heating. Steady or high-frequency wave heating cannot maintain such high temperatures without violating other observational constraints [102,119]. Many studies have detected hot plasma, e.g., [120,121], but the uncertainties are large because the emission is orders of magnitude fainter than that from associated cooler plasma (cf. the review in [122]). Moreover, non-equilibrium ionization effects [123–125] and departures from a Maxwellian distribution due to the presence of accelerated particles [106,126–128] can limit the interpretation of EUV line-emission observations. SXR and HXR thermal bremsstrahlung emissions from the same plasma are not susceptible to non-equilibrium ionization effects, allowing measurements to be more clearly interpreted and the accelerated particles to be more readily detected. The FOXSI-2 sounding rocket performed X-ray measurements of high-temperature plasma in an active region [129], and SXR spectrometers flown on the SDO/EVE sounding rocket [121] and on the MinXSS CubeSat [130] have performed high-temperature measurements of spatially integrated SXR spectra. These measurements provide evidence of impulsive magnetic reconnection events contributing to active-region heating [131]. SPARK will provide important constraints on competing scenarios of coronal heating in active regions [132,133] and directly measure the predicted high-temperature X-ray signature of low-frequency nanoflare heating, improved by observations of multiple coronal emission lines from many ionisation states of Fe. Some of these lines also allow for diagnostics of accelerated electrons [126,128]. Ionization and recombination time scales will be derived through observations of the density of hot plasma, a key measurement not provided by prior EUV observations/missions. SPARK will also provide measurements of magnetic field strengths in active region loops, using the magnetically induced transition at 257.3 Å (c.f. [134] and references therein).

## 2. Payload

SPARK utilises three scientific instruments to provide imaging spectroscopy in the  $\gamma$ -ray, X-ray, and EUV regimes: LISSAN, FOXSI, and SISA, respectively. Figure 3 shows a model of the spacecraft, highlighting the accommodation of the three scientific instruments.

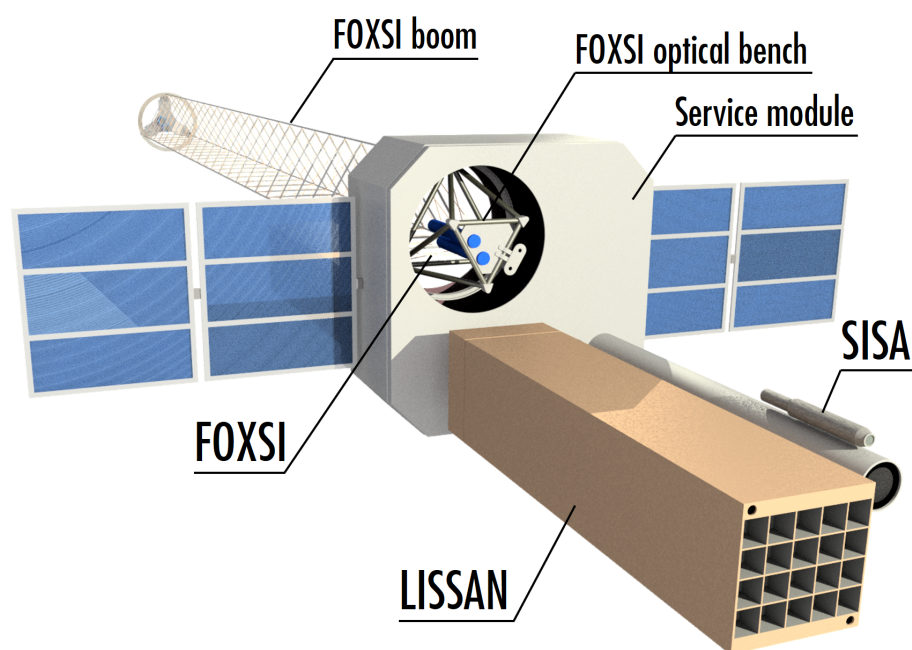


**Figure 3.** SPARK spacecraft model illustrating the payload accommodations.

### 2.1. Large Imaging Spectrometer for Solar Accelerated Nuclei (LISSAN)

LISSAN will, for the first time, reveal the dynamics of accelerated ions in solar flares via spectroscopic imaging between 40 keV and 100 MeV on time scales of less than 10 s. These capabilities will also allow it to observe high-energy X-ray emissions from energetic electrons, providing diagnostics for both types of accelerated particles. This will be achieved by using high-resolution scintillators with an energy resolution of 0.1 MeV at 6.1 MeV and an angular resolution of 8" FWHM. At 6.1 MeV, LISSAN will achieve 40x RHESSI's sensitivity (5 photons/cm<sup>2</sup>) and a spectral resolution of 1.5% dE/E. LISSAN will also achieve 40x RHESSI's sensitivity (50 photons/cm<sup>2</sup>) in the 2.2 MeV neutron capture line. A summary of the predicted performance of LISSAN is presented in Table 1.

**Table 1.** LISSAN instrument performance.

LISSAN Parameter	Expected Performance
Energy Range—Low	40 keV
Energy Range—High	100 MeV
Imaging Effective Area (2.2 MeV)	100 cm <sup>2</sup>
Spectro Effective Area (2.2 MeV)	440 cm <sup>2</sup>
Sensitivity (2.2 MeV)	50 photons/cm <sup>2</sup>
Sensitivity (6.1 MeV)	5 photons/cm <sup>2</sup>
Imaging Time Resolution	1 s
Angular Resolution	8"
Field of View	12.8' diameter
Energy Resolution (6.1 MeV)	1.5% dE/E
Largest Observable Flare	>X5

LISSAN employs an indirect Fourier imaging technique [135,136]. Pairs of 1D slotted grids (bigrids) encode spatial information into moiré patterns, each of which is measured by a pixelated, spectroscopic, photon-counting  $\gamma$ -ray detector. Each bigrid samples an angular scale along a single direction on the plane of the sky. The resulting moiré patterns therefore represent spatial Fourier components of the field of view (visibilities), which can be combined into images via Fourier-based image reconstruction algorithms similar to those used in radio interferometry. This imaging concept has been successfully demonstrated by Solar Orbiter/STIX [22,137] in the 4–150 keV spectral range. LISSAN is composed of 20 subcollimators, 15 of which contain bigrids for imaging spectroscopy. The angular scales and directions they sample depend on the pitch (slit width) and orientation of the bigrids. The resulting visibilities can be represented as complex numbers on the  $(u, v)$  plane. One possible visibility configuration is displayed in the left panel of Figure 4, with its associated point-spread function in the central panel. The right panel shows an image of the 31 March 2022 M9.7 flare that LISSAN would have produced with this configuration in the 50–84 keV range using the CLEAN image reconstruction algorithm. Two non-thermal footpoint sources are clearly visible.

Of LISSAN's five remaining gridless subcollimators, one monitors the background, and four are used to boost sensitivity for spectroscopy. This is because the absence of bigrids increases the photon throughput by a factor four.

The detector of each subcollimator comprises 16 "fingers" of crystal. In one direction, this segmentation allows the moiré pattern to be measured. The other improves light collection and, therefore, spectral resolution and provides a redundant measurement of the moiré pattern. This guarantees the energy resolution needed to measure the Doppler profiles of the C and O lines at 4.4 and 6.1 MeV, respectively.

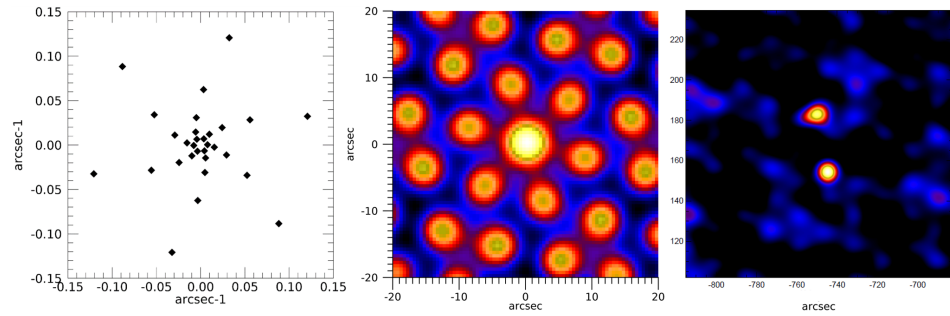


**Figure 4.** Left: One possible  $(u, v)$ -coverage for LISSAN; middle: associated point-spread function (dirty map of a point source on axis; this image contains both the X-ray source and instrumental artefacts to be removed with adequate cleaning algorithms); right: simulation of a LISSAN image of the 50–84 keV emission from the two hard X-ray footpoints during the M9.7 flare on 31 March 2022, which was observed by STIX on Solar Orbiter. This image was obtained by running the CLEAN algorithm on the dirty image.

2.2. Focusing Optics X-ray Solar Imager (FOXSI)

FOXSI combines grazing-incidence hard X-ray focusing optics with small, fast, pixelated detectors to produce images of the Sun at high spectral, spatial, and temporal resolution over the spectral range of 3–50 keV [138]. This strategy offers dramatic improvements in image quality, dynamic range, and sensitivity over the indirect (Fourier-based) imaging techniques of current and previous state-of-the-art solar X-ray spectroscopic imagers, e.g., RHESSI and Solar Orbiter/STIX. FOXSI will be able to reliably image faint thermal and non-thermal sources in the solar corona, even in the presence of brighter ones, for the first time. Such images will enable FOXSI to elucidate a ground-breaking new understanding of particle acceleration and the evolution of solar eruptive events. FOXSI will not intrinsically integrate images over preset time or energy intervals but instead record the energy, position, and arrival time of individual photons, allowing images and spectra to be produced ex post facto in accordance with specific science goals. FOXSI’s design and measurement strategies have been proven through successful flights of several solar sounding rocket and balloon instruments [139–144]. Moreover, FOXSI will build on the success of non-solar space-based direct-focusing X-ray imagers (e.g., NuSTAR and Hitomi) and optimised for the resolution requirements and high fluxes of solar observations. This is achieved via judicious design of the optics’ effective area, fast-counting detectors, and movable attenuators that can be deployed during the largest flares. This prevents corruption of the measured spectrum, e.g., via pile up, which is common in observations of even small solar flares by non-solar telescopes, e.g., NuSTAR. A summary of the predicted performance of FOXSI is presented in Table 2.

**Table 2.** Expected performance of SPARK/FOXSI.

FOXSI Parameter	Expected Performance
Energy Range—Low	3 keV
Energy Range—High	55 keV
Imaging Dynamic Range 1	20:1 beyond 20'' separation
Imaging Dynamic Range 2	1000:1 beyond 45'' separation
Effective Area (at 20 keV)	40 cm <sup>2</sup>
Sensitivity	0.2 photons/cm <sup>2</sup>
Imaging Time Resolution	0.1 s
Angular Resolution	6.3'' FWHM
Field of View	9.8' × 9.8'
Energy Resolution	0.8 keV FWHM
Largest Observable Flare	>X10

FOXSI also includes a soft X-ray spectrometer (FOXSI-STC) that provides spatially integrated high-resolution spectra (0.2 keV FWHM at 1.5 keV) in the range of 0.8–15 keV. The combination of emission lines and thermal continuum emissions in this energy range provides additional plasma temperature and composition information averaged over all the plasma in the FOXSI FOV that FOXSI cannot access to due to its lower energy resolution (0.8 keV) and higher low-energy cutoff (3 keV). FOXSI-STC is composed of two identical spectrometers with different apertures optimised for low and high flux, respectively. This enables it to measure the X-ray fluxes of even the largest flares. FOXSI-STC will be used to control the movable attenuators of FOXSI's HXR focusing telescopes. This approach enables fewer attenuator motions compared to past and current instruments, which have to frequently remove their attenuators for short periods of time (i.e., peek) to check whether the flux has reduced to an acceptable level. A summary of the predicted performance of FOXSI-STC is presented in Table 3.

**Table 3.** Expected performance of SPARK/FOXSI-STC.

FOXSI-STC Parameter	Expected Performance
Energy Range—Low	0.8 keV
Energy Range—High	15 keV
Effective Area	0.01 cm <sup>2</sup>
Energy Resolution	0.2 keV FWHM below 1.5 keV
Field of View	9.8' × 9.8'
Time Resolution	0.5 s
Largest Observable Flare	>X10

### 2.3. Spectral Imager of the Solar Atmosphere (SISA)

SISA (Spectral Imager of the Solar Atmosphere) is an integral field spectrograph (IFS) [145], providing the simultaneous spectra of a bidimensional field of view of 100 arcseconds by 250 arcseconds using image slicer technology. Two spectral ranges will be covered, centred around 18.5 nm and 25 nm, with 1 arcsecond spatial resolution and a spectral resolving power of  $R \sim 3650$ –5160. A spectral ranges of 170–195 Å and 245–260 Å are required to measure the parameters of 1 MK plasma and the hotter 15 MK plasma, respectively. This wavelength range includes lines sensitive to coronal magnetic field strength (Fe X 25.7 nm; see, e.g., [134,146,147]) that can be deduced using a ratio of magnetically sensitive Fe X lines formed at 1 MK. The wavelength range also includes lines sensitive to electron temperature/non-Maxwellian electron distributions [148,149]. It also has a wide range of lines to measure electron densities from coronal (e.g., Fe IX, Fe XI, Fe XII, Fe XV, and Ca XV) to flare temperatures (Fe XXI) and the FIP bias. It observes He II and a wide range of lines, many at flare temperatures (e.g., Fe XVII, Fe XX, Fe XXI, Fe XXII, Fe XXIII, and Fe XXIV).

In order to achieve the temporal resolution of 1 second required to capture the rapid development of the plasma environment during flare energy release, the simultaneous observation of a 2D field of view without the traditional use of slit scanning systems is a key factor. The integral field spectroscopy technique is a novel proposal for the extreme ultraviolet (EUV) regime and benefits from a wide heritage of integral field spectrographs operating in ground-based and space-based telescopes. This strategy has significant advantages over traditional EUV scanning spectroscopy (e.g., EIS, IRIS, and Solar-C/EUVST), making 2D images over two orders of magnitude faster than before. The wavelength range of SISA is both different and wider than that of the upcoming Multi-Slit Solar Explorer (MUSE; [26]) spacecraft, offering a wide array of plasma diagnostics so that 2D maps of, for example, electron density (at multiple temperatures) and the magnetic field will be obtained. We note that several SISA diagnostic, such as the measurements of coronal magnetic fields and departures from electron Maxwellian distributions, are not available to SOLAR-C/EUVST. A summary of the predicted performance of SISA is presented in Table 4. The ability to obtain diagnostics at 1 s cadence is based on estimates of the signal

in active region cores and flares and the strawman design (described in the SISA paper), consisting of a single multilayer for the three reflecting surfaces and a 20 cm aperture of the off-axis telescope.

SISA will be composed of two subsystems: the telescope, an off-axis parabolic mirror; and the integral field spectrograph, an array of curved slicer mirrors and curved gratings. The slicer mirrors are placed at the telescope focus and decompose (slice) the image of the field of view using an array of powered rectangular mirrors, each with a different tilt angle around the X and Y axes. These will produce a pupil image per slice reflected in different directions towards the curved gratings, which perform three functions: (i) dispersion of the incoming beam into its constituent wavelengths, (ii) imaging of the beams on the detector with the required magnification, and (iii) control of the location of the exit pupil. The orientations of the gratings are fixed. Each grating will produce the spectrum of each slice of the field, as shown in Figure 5. The tilt of each grating will be defined to distribute the spectra on the detectors. SISA will be the first integral field spectrograph in the EUV spectral range.

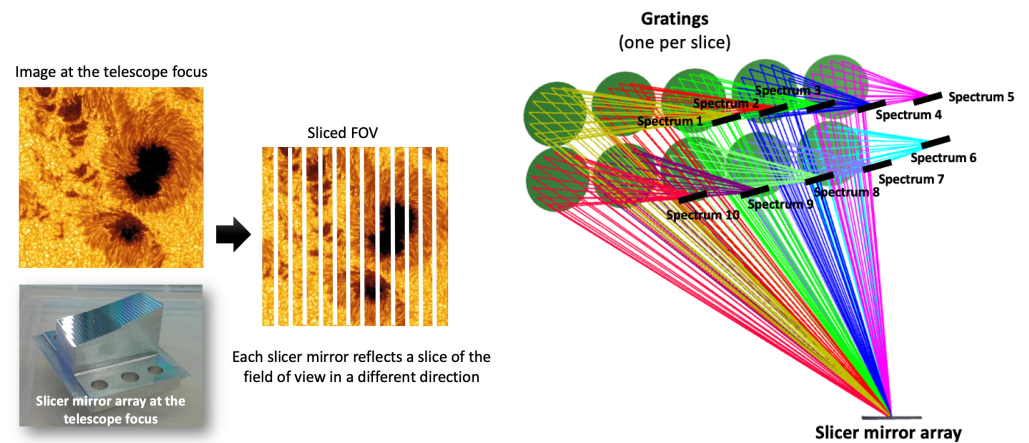


**Figure 5.** Left: Sketch of the functionality of an image slicer. The image slicer acts as a field reformatter, slicing the entrance field of view and generating one pupil per slice (Note that despite apparent gaps in the sliced FOV in the figure, it provides a contiguous map when combined). Right: SISA conceptual layout with a reduced number of slicers. Each curved grating produces the spectrum of each slice of the field. The tilt angles of the gratings offer flexibility in the geometrical distribution of the spectra on the detector.

**Table 4.** Instrument requirements and expected performance of SISA.

SISA Parameter	Expected Performance
Spectral Window 1	178–184 Å
Spectral Window 2	221–264 Å
Spectral Resolution	0.05 Å FWHM
Spectral Resolving Power (R)	3560–5160
Field of View	100'' × 250''
Spatial Resolution	1'' in 2 pixels
Temporal Resolution (high signal)	1 s
Temporal Resolution (low signal)	10 s

#### 2.4. Mass and Power

The required resources for LISSAN, FOXSI (including FOXSI-STC), and SISA are given in Table 5. The mass estimates include a 20% margin on each instrument, whilst the power requirements include a 30% margin on each instrument. The operating temperatures are the most stringent constraints for each instrument; particularly relevant are the front-end electronics (FEE) for LISSAN and the focal-plane assembly (FPA) for both FOXSI and SISA.

**Table 5.** Required resources for LISSAN, FOXSI (including FOXSI-STC), and SISA.

Resource	LISSAN	FOXSI	SISA
Mass	370 kg	120 kg	78 kg
Volume	1.96 m <sup>3</sup>	(105 cm) <sup>3</sup> (stowed)	0.5 m <sup>3</sup>
Power	125 W (peak)	170 W (average)	130 W (average)
Data Rate	25 Mbits/s (peak)	1 Mbits/s (peak)	50 Mbits/s (average)
Operating Temp.	0 °C (FEE)	−20–0 °C (FPA)	<−40 °C (FPA)

### 3. Proposed Mission Configuration and Profile

To meet its science objectives, SPARK must be launched at a time when medium-to-large solar flares can be observed. This can be achieved at any time in the solar cycle except solar minimum.

#### 3.1. System-Level Requirements

The overlapping fields of view (FOV) of LISSAN, FOXSI and SISA are shown in Figure 6. A pointing accuracy of 10 arcsecs is required due to the FOV of all of SPARK's instruments and the need to point to a chosen active region. The performance drift error (PDE) is driven by the spatial resolution of SISA and is 0.1 arcsec within a time interval of one second. The requirement will be fulfilled by further attenuating the spacecraft PDE with a tip/tilt system. Each instrument suite will carry its own aspect system to overcome uncertainty in coalignment between the instruments, as the precise knowledge of the positions of the  $\gamma$ -ray, X-ray, and EUV emissions relative to one another is key to fulfilling the scientific objectives of the mission. Therefore, each instrument will provide precise knowledge of the pointing.

LISSAN and the FOXSI HXR telescopes will operate in one nominal observing mode. SISA will have two operational modes. The first mode (cadence 1) will be for observing flaring active regions when there is an abundance of EUV radiation. The second mode (cadence 2) is optimised for weaker signals when the Sun is less active, requiring slower exposure times. A safe mode will be implemented for each instrument to react to instrument or spacecraft failure.

#### 3.2. Operations

The SPARK payload is designed to provide synchronized observations that address specific science questions. Since the instruments will always observe the same targets, the science operations will not require a large degree of flexibility. As instruments have a FOV smaller than the full Sun, target selection will be required. Targets will typically be solar active regions most likely to produce energetic flares. SPARK will allow the community to submit observing plans for targeted observations.

Science and housekeeping data recorded in the onboard mass memory will be brought down in raw format for processing on the ground into level 0 format. The nature of multiple downlink stations may require that data be aggregated and sorted before this processing. Further pipeline processing will bring data to level-2-derived products via level-1-calibrated data. Minimal data processing will happen on board, and all the data will be downlinked for processing on the ground.

#### 3.3. Spacecraft Design

The primary drivers for the SPARK spacecraft design are the accommodation of the extendable boom for FOXSI and the large mass of LISSAN. The boom will be deployed in orbit, and alignment between the optics on the spacecraft and the detectors at the tip of the extendable structure will be performed using the FOXSI tip/tilt mechanism.

SPARK's payload includes imaging instruments and therefore requires a three-axis system to minimise spatial blurring. The combination of individual instrument stability requirements leads to an overall requirement for the PDE of 0.1'' over 1 second. The

spacecraft absolute performance error (APE) is  $10''$  to allow a 10% error on the smaller SISA field of view pointing at the correct target. The requirement for the relative performance error (RPE) is  $1''$  for integration times of 1 s. The attitude sensors should include a fine Sun sensor and a star tracker in order to determine spacecraft pointing relative to the Sun. An inertial reference unit is required to determine changes in attitude over time.

SPARK's baseline L1 orbit provides a stable thermal environment such that the thermal control on the instruments can maintain any required temperature. The spacecraft will have one side constantly facing the Sun and one side facing cold space all the time. SPARK's thermal requirements can be met by a passive cooling system consisting of cold fingers and radiators.

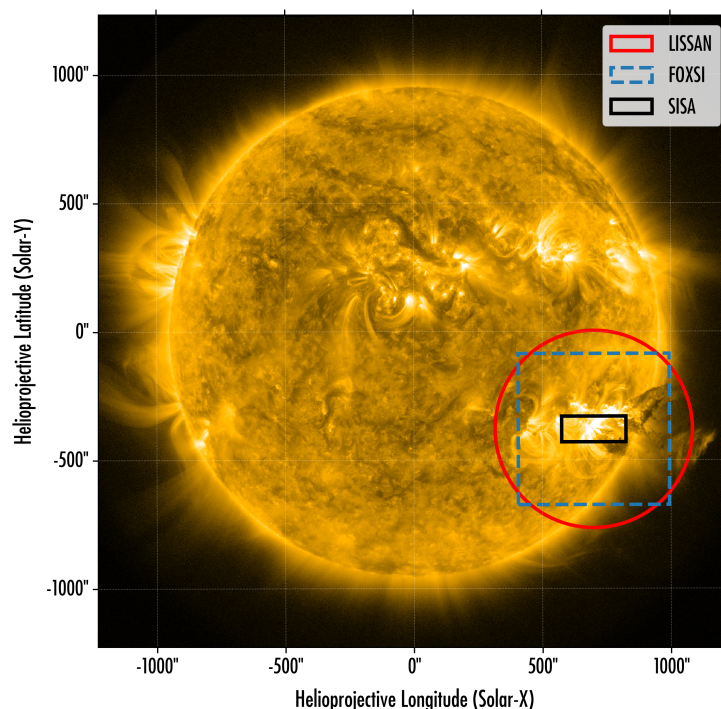


**Figure 6.** Fields of view of the three imaging instruments of SPARK overplotted on the EUV 171 Å Sun from AIA.

SPARK will provide science data downlink to Earth using a K-band 26 GHz antenna. Even with a reduced ground station contact of 4 hours to obtain 850 Gbits/day (similar to Euclid), this would be enough to downlink the entire maximum daily data volumes of 80 Gbit (LISSAN) and 86 Gbit (FOXSI). The SISA maximum daily data volume of 4.3 Tbits/day would be stored using onboard mass memory storage of at least 4 TB, with synoptic data being communicated to the Earth to choose a subset of events to download and/or periods to downlink with reduced cadence.

#### 4. Current Status of SPARK

SPARK was initially submitted to the ESA in 2010 as an M-class mission proposal that included a modified version of LISSAN and FOXSI with different supporting instruments. More recently, the relevant particle acceleration and transport topical questions were presented as an ESA Voyage 2050 white paper in 2020 and subsequently published [150].

SPARK in its current form was proposed to the ESA in 2022 as an M-class mission and reached Phase-2. Development of the individual instruments proposed for SPARK continues, funded by national efforts. The United Kingdom is developing EUV image slicer technology for SISA, France is developing X-ray detectors for FOXSI, Germany is developing grids for LISSAN, and Belgium is developing improved detectors for SISA.

There is clear support for the goals and implementation of SPARK across the broad European scientific community in solar physics and beyond. The implementation of SPARK in this form presents an exciting opportunity for paradigm-shifting observations in the field of astrophysical particle acceleration and transport, using data from our local laboratory, the Sun.

**Author Contributions:** The writing of this paper was led by H.A.S.R. The paper was based upon the SPARK mission concept that was coordinated by H.A.S.R., S.M. (Sophie Musset), and D.F.R. All other authors contributed by providing scientific expertise or instrumentation expertise in the development of the LISSAN, FOXSI, and SISA concepts and/or the paper itself. All authors have read and agreed to the published version of the manuscript.

**Funding:** H.A.S.R. and S.A.M. were funded by the Science, Technology, and Facilities Council (STFC) under consolidated grant ST/W001004/1. D.M.L. is grateful to the STFC award of an Ernest Rutherford Fellowship (ST/R003246/1). Jaroslav Dudík was funded by the Czech National Science Foundation (Grant No. GACR 22-07155S). Jaroslav Dudík and J.K. were supported by project RWO:67985815. D.O.S. acknowledges financial support from through grants AEI/MCIN/10.13039/501100011033/(RTI2018-096886-C5, PID2021-125325OB-C5, PCI2022-135009-2), and ERDF “A way of making Europe” and “Center of Excellence Severo Ochoa” awards to IAA-CSIC (CEX2021-001131-S). S.M. and T.M. were supported by the National Science Centre, Poland (Grant No. 2020/39/B/ST9/01591). G.S.K. acknowledges financial support from NASA’s Early Career Investigator Program (Grant No. NASA 80NSSC21K0460). G.D.Z. acknowledges support from STFC (UK) via the consolidated grants to the atomic astrophysics group at DAMTP, University of Cambridge (ST/P000665/1. and ST/T000481/1).

**Data Availability Statement:** No new data were created or analyzed in this study. Data sharing is not applicable to this article.

**Acknowledgments:** The concept for the FOXSI instrument on board SPARK was based upon the extensive work that was carried out by the FOXSI SMEX team [138] and by the FIERCE team (see <https://doi.org/10.5281/zenodo.3674078>). Figures 1 and 2 are from the work carried out by both these teams.

**Conflicts of Interest:** The authors declare no conflict of interest.

## Abbreviations

The following abbreviations are used in this manuscript:

AIA	Atmospheric imaging assembly
CME	Coronal mass ejection
EIS	EUV Imaging Spectrometer on board Hinode
EUV	Extreme ultraviolet
EUVST	Extreme Ultraviolet High-Throughput Spectroscopic Telescope
EVE	EUV Variability Experiment on board SDO
FEE	Front-end electronics
FIERCE	Fundamentals of Impulsive Energy Release in the Corona Explorer
FPA	Focal-plane assembly
FOV	Field of view
FOXSI	Focusing Optics X-ray Solar Imager
FOXSI-STC	FOXSI’s Spectrometer for Temperature and Composition
FWHM	Full-width half maximum
GOES	Geostationary Operational Environmental Satellite
HXR	Hard X-ray
IFS	Integral field spectrograph
IRIS	Interface Region Imaging Spectrograph
LISSAN	Large Imaging Spectrometer for Solar Accelerated Nuclei
MHD	Magnetohydrodynamic
MUSE	Multi-Slit Solar Explorer
NuSTAR	Nuclear Spectroscopic Telescope Array

RHESSI	Reuven Ramaty High-Energy Solar Spectroscopic Imager
SDO	Solar Dynamics Observatory
SEP	Solar energetic particle
SISA	Spectral Imager of the Solar Atmosphere
SPARK	Solar Particle Acceleration, Radiation, and Kinetics mission
STIX	Spectrometer/Telescope for Imaging X-rays
SXR	Soft X-ray

## References

- Shibata, K. New observational facts about solar flares from YOHKOH studies—Evidence of magnetic reconnection and a unified model of flares. *Adv. Space Res.* **1996**, *17*, 9–18. [\[CrossRef\]](#)
- Brown, J.C. The Deduction of Energy Spectra of Non-Thermal Electrons in Flares from the Observed Dynamic Spectra of Hard X-Ray Bursts. *Sol. Phys.* **1971**, *18*, 489–502. [\[CrossRef\]](#)
- Piana, M.; Massone, A.M.; Kontar, E.P.; Emslie, A.G.; Brown, J.C.; Schwartz, R.A. Regularized Electron Flux Spectra in the 2002 July 23 Solar Flare. *Astrophys. J. Lett.* **2003**, *595*, L127–L130. [\[CrossRef\]](#)
- Holman, G.D.; Aschwanden, M.J.; Aurass, H.; Battaglia, M.; Grigis, P.C.; Kontar, E.P.; Liu, W.; Saint-Hilaire, P.; Zharkova, V.V. Implications of X-ray Observations for Electron Acceleration and Propagation in Solar Flares. *Space Sci. Rev.* **2011**, *159*, 107–166. [\[CrossRef\]](#)
- Kontar, E.P.; Brown, J.C.; Emslie, A.G.; Hajdas, W.; Holman, G.D.; Hurford, G.J.; Kašparová, J.; Mallik, P.C.V.; Massone, A.M.; McConnell, M.L.; et al. Deducing Electron Properties from Hard X-ray Observations. *Space Sci. Rev.* **2011**, *159*, 301–355. [\[CrossRef\]](#)
- Benz, A.O. Flare Observations. *Living Rev. Sol. Phys.* **2017**, *14*, 2. [\[CrossRef\]](#)
- Chupp, E.L. High-Energy Neutral Radiations from the Sun. *Annu. Rev. Astron Astrophys.* **1984**, *22*, 359–387. [\[CrossRef\]](#)
- Ramaty, R. Nuclear processes in solar flares. In *Physics of the Sun: Volume II: The Solar Atmosphere*; Springer: Dordrecht, The Netherlands, 1986; Volume 2, pp. 291–323.
- Chupp, E.L. Evolution of our understanding of solar flare particle acceleration: (1942–1995). In *High Energy Solar Physics*; Ramaty, R., Mandzhavidze, N., Hua, X.M., Eds.; American Institute of Physics Conference Series; American Institute of Physics: College Park, MD, USA, 1996; Volume 374, pp. 3–34. [\[CrossRef\]](#)
- Trottet, G.; Vilmer, N. The Production of Flare-Accelerated Particles at the Sun. In *European Meeting on Solar Physics*; Simnett, G.M., Alissandrakis, C.E., Vlahos, L., Eds.; Springer: Berlin/Heidelberg, Germany, 1997; Volume 489, p. 219. [\[CrossRef\]](#)
- Share, G.H.; Murphy, R.J. Gamma Ray Spectroscopy in the Pre-HESSI Era. In *High Energy Solar Physics Workshop—Anticipating Hess!*; Ramaty, R., Mandzhavidze, N., Eds.; Astronomical Society of the Pacific Conference Series; American Institute of Physics: College Park, MD, USA, 2000; Volume 206, p. 377.
- Vilmer, N.; MacKinnon, A.L.; Trottet, G.; Barat, C. High energy particles accelerated during the large solar flare of 1990 May 24: X/ $\gamma$ -ray observations. *Astron. Astrophys.* **2003**, *412*, 865–874. [\[CrossRef\]](#)
- Share, G.H.; Murphy, R.J. Gamma Radiation From Flare-Accelerated Particles Impacting the Sun. *Geophys. Monogr. Ser.* **2006**, *165*, 177. [\[CrossRef\]](#)
- Vilmer, N.; MacKinnon, A.L.; Hurford, G.J. Properties of Energetic Ions in the Solar Atmosphere from  $\gamma$ -Ray and Neutron Observations. *Space Sci. Rev.* **2011**, *159*, 167–224. [\[CrossRef\]](#)
- Stecker, F.W. The Cosmic  $\gamma$ -Ray Spectrum from Secondary Particle Production in Cosmic-Ray Interactions. *Astrophys. Space Sci.* **1970**, *6*, 377–389. [\[CrossRef\]](#)
- Murphy, R.J.; Dermer, C.D.; Ramaty, R. High-Energy Processes in Solar Flares. *Astrophys. J. Suppl.* **1987**, *63*, 721. [\[CrossRef\]](#)
- Hurford, G.J.; Schwartz, R.A.; Krucker, S.; Lin, R.P.; Smith, D.M.; Vilmer, N. First Gamma-Ray Images of a Solar Flare. *Astrophys. J. Lett.* **2003**, *595*, L77–L80. [\[CrossRef\]](#)
- Ramaty, R.; Mandzhavidze, N. High energy processes in solar flares. In *Proceedings of the Cosmic Explosions: Tenth Astrophysics Conference*, College Park, MD, USA, 11–13 October 1999; Holt, S.S., Zhang, W.W., Eds.; American Institute of Physics Conference Series; American Institute of Physics: College Park, MD, USA, 2000; Volume 522, pp. 401–410. [\[CrossRef\]](#)
- Emslie, A.G.; Dennis, B.R.; Shih, A.Y.; Chamberlin, P.C.; Mewaldt, R.A.; Moore, C.S.; Share, G.H.; Vourlidas, A.; Welsch, B.T. Global Energetics of Thirty-eight Large Solar Eruptive Events. *Astrophys. J.* **2012**, *759*, 71. [\[CrossRef\]](#)
- Aschwanden, M.J.; Caspi, A.; Cohen, C.M.S.; Holman, G.; Jing, J.; Kretzschmar, M.; Kontar, E.P.; McTiernan, J.M.; Mewaldt, R.A.; O’Flannagain, A.; et al. Global Energetics of Solar Flares. V. Energy Closure in Flares and Coronal Mass Ejections. *Astrophys. J.* **2017**, *836*, 17. [\[CrossRef\]](#)
- Lin, R.P.; Dennis, B.R.; Hurford, G.J.; Smith, D.M.; Zehnder, A.; Harvey, P.R.; Curtis, D.W.; Pankow, D.; Turin, P.; Bester, M.; et al. The Reuven Ramaty High-Energy Solar Spectroscopic Imager (RHESSI). *Sol. Phys.* **2002**, *210*, 3–32. [\[CrossRef\]](#)
- Krucker, S.; Hurford, G.J.; Grimm, O.; Kögl, S.; Gröbelbauer, H.P.; Etesi, L.; Casadei, D.; Csillaghy, A.; Benz, A.O.; Arnold, N.G.; et al. The Spectrometer/Telescope for Imaging X-rays (STIX). *Astron. Astrophys.* **2020**, *642*, A15. [\[CrossRef\]](#)
- Culhane, J.L.; Harra, L.K.; James, A.M.; Al-Janabi, K.; Bradley, L.J.; Chaudry, R.A.; Rees, K.; Tandy, J.A.; Thomas, P.; Whillock, M.C.R.; et al. The EUV Imaging Spectrometer for Hinode. *Sol. Phys.* **2007**, *243*, 19–61. [\[CrossRef\]](#)

24. SPICE Consortium; Anderson, M.; Appourchaux, T.; Auchère, F.; Aznar Cuadrado, R.; Barbay, J.; Baudin, F.; Beardsley, S.; Bocchialini, K.; Borgo, B.; et al. The Solar Orbiter SPICE instrument. An extreme UV imaging spectrometer. *Astron. Astrophys.* **2020**, *642*, A14. [[CrossRef](#)]
25. Shimizu, T.; Imada, S.; Kawate, T.; Suematsu, Y.; Hara, H.; Tsuzuki, T.; Katsukawa, Y.; Kubo, M.; Ishikawa, R.; Watanabe, T.; et al. The Solar-C (EUVST) mission: The latest status. In *Space Telescopes and Instrumentation 2020: Ultraviolet to Gamma Ray*; den Herder, J.W.A., Nikzad, S., Nakazawa, K., Eds.; Society of Photo-Optical Instrumentation Engineers (SPIE) Conference Series; SPIE: Bellingham, WA, USA, 2020; Volume 11444, p. 114440N. [[CrossRef](#)]
26. De Pontieu, B.; Martínez-Sykora, J.; Testa, P.; Winebarger, A.R.; Daw, A.; Hansteen, V.; Cheung, M.C.M.; Antolin, P. The Multi-slit Approach to Coronal Spectroscopy with the Multi-slit Solar Explorer (MUSE). *Astrophys. J.* **2020**, *888*, 3. [[CrossRef](#)]
27. De Pontieu, B.; Testa, P.; Martínez-Sykora, J.; Antolin, P.; Karampelas, K.; Hansteen, V.; Rempel, M.; Cheung, M.C.M.; Reale, F.; Danilovic, S.; et al. Probing the Physics of the Solar Atmosphere with the Multi-slit Solar Explorer (MUSE). I. Coronal Heating. *Astrophys. J.* **2022**, *926*, 52. [[CrossRef](#)]
28. Cheung, M.C.M.; Martínez-Sykora, J.; Testa, P.; De Pontieu, B.; Chintzoglou, G.; Rempel, M.; Polito, V.; Kerr, G.S.; Reeves, K.K.; Fletcher, L.; et al. Probing the Physics of the Solar Atmosphere with the Multi-slit Solar Explorer (MUSE). II. Flares and Eruptions. *Astrophys. J.* **2022**, *926*, 53. [[CrossRef](#)]
29. Aschwanden, M.J.; Kontar, E.P.; Jeffrey, N.L.S. Global Energetics of Solar Flares. VIII. The Low-energy Cutoff. *Astrophys. J.* **2019**, *881*, 1. [[CrossRef](#)]
30. Drake, J.F.; Swisdak, M.; Che, H.; Shay, M.A. Electron acceleration from contracting magnetic islands during reconnection. *Nature* **2006**, *443*, 553–556. [[CrossRef](#)] [[PubMed](#)]
31. Arnold, H.; Drake, J.F.; Swisdak, M.; Guo, F.; Dahlin, J.T.; Chen, B.; Fleishman, G.; Glesener, L.; Kontar, E.; Phan, T.; et al. Electron Acceleration during Macroscale Magnetic Reconnection. *Phys. Rev. Lett.* **2021**, *126*, 135101. [[CrossRef](#)] [[PubMed](#)]
32. Miller, J.A.; Cargill, P.J.; Emslie, A.G.; Holman, G.D.; Dennis, B.R.; LaRosa, T.N.; Winglee, R.M.; Benka, S.G.; Tsuneta, S. Critical issues for understanding particle acceleration in impulsive solar flares. *J. Geophys. Res.* **1997**, *102*, 14631–14660. [[CrossRef](#)]
33. Petrosian, A.R.; Boulesteix, J.; Comte, G.; Kunth, D.; Lecoarer, E. An interferometric study of the blue compact dwarf galaxy IZW 18. *Astron. Astrophys.* **1997**, *318*, 390–404.
34. Vlahos, L.; Anastasiadis, A.; Papaioannou, A.; Kouloumvakos, A.; Isliker, H. Sources of solar energetic particles. *Philos. Trans. R. Soc. Lond. Ser. A* **2019**, *377*, 20180095. [[CrossRef](#)]
35. Vlahos, L.; Isliker, H. Particle acceleration and heating in a turbulent solar corona. *Plasma Phys. Control. Fusion* **2019**, *61*, 014020. [[CrossRef](#)]
36. Kiener, J.; Gros, M.; Tatischeff, V.; Weidenspointner, G. Properties of the energetic particle distributions during the October 28, 2003 solar flare from INTEGRAL/SPI observations. *Astron. Astrophys.* **2006**, *445*, 725–733. [[CrossRef](#)]
37. Litvinenko, Y.E.; Craig, I.J.D. Flare Energy Release by Flux Pile-up Magnetic Reconnection in a Turbulent Current Sheet. *Astrophys. J.* **2000**, *544*, 1101–1107. [[CrossRef](#)]
38. Holman, G.D.; Benka, S.G. A Hybrid Thermal/Nonthermal Model for the Energetic Emissions from Solar Flares. *Astrophys. J. Lett.* **1992**, *400*, L79. [[CrossRef](#)]
39. Alexander, W.M.; Tanner, W.G.; McDonald, R.A.; Schaub, G.E.; Stephenson, S.L.; McDonnell, J.A.M.; Maag, C.R. The Status of Measurement Technologies Concerning Micrometer and Submicrometer Space Articulate Matter Capture, Recovery, Velocity, and Trajectory. In *Proceedings of the Particle Capture, Recovery and Velocity/Trajectory Measurement Technologies*, Houston, TX, USA, 27–28 September 1993; Zolensky, M.E., Ed.; p. 11.
40. Dunphy, P.P.; Chupp, E.L.; Bertsch, D.L.; Schneid, E.J.; Gottesman, S.R.; Kanbach, G. Gamma-Rays and Neutrons as a Probe of Flare Proton Spectra: The Solar Flare of 11 June 1991. *Sol. Phys.* **1999**, *187*, 45–57. [[CrossRef](#)]
41. Kocharov, L.G.; Lee, J.W.; Zirin, H.; Kovaltsov, G.A.; Usoskin, I.G.; Pyle, K.R.; Shea, M.A.; Smart, D.F. Neutron and electromagnetic emissions during the 1990 May 24 solar flare. *Sol. Phys.* **1994**, *155*, 149–170. [[CrossRef](#)]
42. Kocharov, L.; Debrunner, H.; Kovaltsov, G.; Lockwood, J.; McConnell, M.; Nieminen, P.; Rank, G.; Ryan, J.; Schoenfelder, V. Deduced spectrum of interacting protons accelerated after the impulsive phase of the 15 June 1991 solar flare. *Astron. Astrophys.* **1998**, *340*, 257–264.
43. Vilmer, N.; Krucker, S.; Trotter, G.; Lin, R.P. Hard X-ray and metric/decimetric spatially resolved observations of the 10 April 2002 solar flare. *Adv. Space Res.* **2003**, *32*, 2509–2515. [[CrossRef](#)]
44. Kanbach, G.; Bertsch, D.L.; Fichtel, C.E.; Hartman, R.C.; Hunter, S.D.; Kniffen, D.A.; Kwok, P.W.; Lin, Y.C.; Mattox, J.R.; Mayer-Hasselwander, H.A. Detection of a long-duration solar gamma-ray flare on June 11, 1991 with EGRET on COMPTON-GRO. *Astron. Astrophys. Suppl.* **1993**, *97*, 349–353.
45. Ryan, J.M.; Lockwood, J.A.; Debrunner, H. Solar Energetic Particles. *Space Sci. Rev.* **2000**, *93*, 35–53. [[CrossRef](#)]
46. Allred, J.C.; Hawley, S.L.; Abbett, W.P.; Carlsson, M. Radiative Hydrodynamic Models of the Optical and Ultraviolet Emission from Solar Flares. *Astrophys. J.* **2005**, *630*, 573–586. [[CrossRef](#)]
47. Allred, J.C.; Kowalski, A.F.; Carlsson, M. A Unified Computational Model for Solar and Stellar Flares. *Astrophys. J.* **2015**, *809*, 104. [[CrossRef](#)]
48. Allred, J.C.; Kerr, G.S.; Gordon Emslie, A. Solar Flare Heating with Turbulent Suppression of Thermal Conduction. *Astrophys. J.* **2022**, *931*, 60. [[CrossRef](#)]

49. Kowalski, A.F.; Hawley, S.L.; Carlsson, M.; Allred, J.C.; Uitenbroek, H.; Osten, R.A.; Holman, G. New Insights into White-Light Flare Emission from Radiative-Hydrodynamic Modeling of a Chromospheric Condensation. *Sol. Phys.* **2015**, *290*, 3487–3523. [[CrossRef](#)]
50. Kowalski, A.F.; Allred, J.C.; Daw, A.; Cauzzi, G.; Carlsson, M. The Atmospheric Response to High Nonthermal Electron Beam Fluxes in Solar Flares. I. Modeling the Brightest NUV Footpoints in the X1 Solar Flare of 2014 March 29. *Astrophys. J.* **2017**, *836*, 12. [[CrossRef](#)]
51. Rubio da Costa, F.; Kleint, L.; Petrosian, V.; Liu, W.; Allred, J.C. Data-driven Radiative Hydrodynamic Modeling of the 2014 March 29 X1.0 Solar Flare. *Astrophys. J.* **2016**, *827*, 38. [[CrossRef](#)]
52. Kerr, G.S.; Fletcher, L.; Russell, A.J.B.; Allred, J.C. Simulations of the Mg II k and Ca II 8542 lines from an Alfvén Wave-heated Flare Chromosphere. *Astrophys. J.* **2016**, *827*, 101. [[CrossRef](#)]
53. Kerr, G.S.; Carlsson, M.; Allred, J.C.; Young, P.R.; Daw, A.N. SI IV Resonance Line Emission during Solar Flares: Non-LTE, Nonequilibrium, Radiation Transfer Simulations. *Astrophys. J.* **2019**, *871*, 23. [[CrossRef](#)]
54. Kerr, G.S.; Allred, J.C.; Polito, V. Solar Flare Arcade Modeling: Bridging the Gap from 1D to 3D Simulations of Optically Thin Radiation. *Astrophys. J.* **2020**, *900*, 18. [[CrossRef](#)]
55. Brown, S.A.; Fletcher, L.; Kerr, G.S.; Labrosse, N.; Kowalski, A.F.; De La Cruz Rodríguez, J. Modeling of the Hydrogen Lyman Lines in Solar Flares. *Astrophys. J.* **2018**, *862*, 59. [[CrossRef](#)]
56. Polito, V.; Testa, P.; Allred, J.; De Pontieu, B.; Carlsson, M.; Pereira, T.M.D.; Gošić, M.; Reale, F. Investigating the Response of Loop Plasma to Nanoflare Heating Using RADYN Simulations. *Astrophys. J.* **2018**, *856*, 178. [[CrossRef](#)]
57. Polito, V.; Testa, P.; De Pontieu, B. Can the Superposition of Evaporative Flows Explain Broad Fe XXI Profiles during Solar Flares? *Astrophys. J. Lett.* **2019**, *879*, L17. [[CrossRef](#)]
58. Zhu, Y.; Kowalski, A.F.; Tian, H.; Uitenbroek, H.; Carlsson, M.; Allred, J.C. Modeling Mg II h, k and Triplet Lines at Solar Flare Ribbons. *Astrophys. J.* **2019**, *879*, 19. [[CrossRef](#)]
59. Reep, J.W.; Polito, V.; Warren, H.P.; Crump, N.A. The Duration of Energy Deposition on Unresolved Flaring Loops in the Solar Corona. *Astrophys. J.* **2018**, *856*, 149. [[CrossRef](#)]
60. Reep, J.W.; Russell, A.J.B. Alfvénic Wave Heating of the Upper Chromosphere in Flares. *Astrophys. J. Lett.* **2016**, *818*, L20. [[CrossRef](#)]
61. Reep, J.W.; Russell, A.J.B.; Tarr, L.A.; Leake, J.E. A Hydrodynamic Model of Alfvénic Wave Heating in a Coronal Loop and Its Chromospheric Footpoints. *Astrophys. J.* **2018**, *853*, 101. [[CrossRef](#)]
62. Reep, J.W.; Bradshaw, S.J.; Crump, N.A.; Warren, H.P. Efficient Calculation of Non-local Thermodynamic Equilibrium Effects in Multithreaded Hydrodynamic Simulations of Solar Flares. *Astrophys. J.* **2019**, *871*, 18. [[CrossRef](#)]
63. Cheung, M.C.M.; Rempel, M.; Chintzoglou, G.; Chen, F.; Testa, P.; Martínez-Sykora, J.; Sainz Dalda, A.; DeRosa, M.L.; Malanushenko, A.; Hansteen, V.; et al. A comprehensive three-dimensional radiative magnetohydrodynamic simulation of a solar flare. *Nat. Astron.* **2019**, *3*, 160–166. [[CrossRef](#)]
64. Hurford, G.J.; Krucker, S.; Lin, R.P.; Schwartz, R.A.; Share, G.H.; Smith, D.M. Gamma-Ray Imaging of the 2003 October/November Solar Flares. *Astrophys. J. Lett.* **2006**, *644*, L93–L96. [[CrossRef](#)]
65. del Zanna, G.; Schmieder, B.; Mason, H.; Berlicki, A.; Bradshaw, S. The Gradual Phase of the X17 Flare on October 28, 2003. *Sol. Phys.* **2006**, *239*, 173–191. [[CrossRef](#)]
66. Milligan, R.O.; Dennis, B.R. Velocity Characteristics of Evaporated Plasma Using Hinode/EUV Imaging Spectrometer. *Astrophys. J.* **2009**, *699*, 968–975. [[CrossRef](#)]
67. Milligan, R.O. Spatially Resolved Nonthermal Line Broadening during the Impulsive Phase of a Solar Flare. *Astrophys. J.* **2011**, *740*, 70. [[CrossRef](#)]
68. Kontar, E.P.; Perez, J.E.; Harra, L.K.; Kuznetsov, A.A.; Emslie, A.G.; Jeffrey, N.L.S.; Bian, N.H.; Dennis, B.R. Turbulent Kinetic Energy in the Energy Balance of a Solar Flare. *Phys. Rev. Lett.* **2017**, *118*, 155101. [[CrossRef](#)] [[PubMed](#)]
69. Nakariakov, V.M.; Melnikov, V.F. Quasi-Periodic Pulsations in Solar Flares. *Space Sci. Rev.* **2009**, *149*, 119–151. [[CrossRef](#)]
70. McLaughlin, J.A.; Nakariakov, V.M.; Dominique, M.; Jelínek, P.; Takasao, S. Modelling Quasi-Periodic Pulsations in Solar and Stellar Flares. *Space Sci. Rev.* **2018**, *214*, 45. [[CrossRef](#)]
71. Zimovets, I.V.; McLaughlin, J.A.; Srivastava, A.K.; Kolotkov, D.Y.; Kuznetsov, A.A.; Kupriyanova, E.G.; Cho, I.H.; Inglis, A.R.; Reale, F.; Pascoe, D.J.; et al. Quasi-Periodic Pulsations in Solar and Stellar Flares: A Review of Underpinning Physical Mechanisms and Their Predicted Observational Signatures. *Space Sci. Rev.* **2021**, *217*, 66. [[CrossRef](#)]
72. Nakariakov, V.M.; Kolotkov, D.Y.; Kupriyanova, E.G.; Mehta, T.; Pugh, C.E.; Lee, D.H.; Broomhall, A.M. Non-stationary quasi-periodic pulsations in solar and stellar flares. *Plasma Phys. Control. Fusion* **2019**, *61*, 014024. [[CrossRef](#)]
73. Hayes, L.A.; Inglis, A.R.; Christe, S.; Dennis, B.; Gallagher, P.T. Statistical Study of GOES X-Ray Quasi-periodic Pulsations in Solar Flares. *Astrophys. J.* **2020**, *895*, 50. [[CrossRef](#)]
74. Emslie, A.G.; Sturrock, P.A. Temperature minimum heating in solar flares by resistive dissipation of Alfvén waves. *Sol. Phys.* **1982**, *80*, 99–112. [[CrossRef](#)]
75. Fletcher, L.; Hudson, H.S. Impulsive Phase Flare Energy Transport by Large-Scale Alfvén Waves and the Electron Acceleration Problem. *Astrophys. J.* **2008**, *675*, 1645–1655. [[CrossRef](#)]
76. Russell, A.J.B.; Fletcher, L. Propagation of Alfvénic Waves from Corona to Chromosphere and Consequences for Solar Flares. *Astrophys. J.* **2013**, *765*, 81. [[CrossRef](#)]

77. Laming, J.M. The FIP and Inverse-FIP Effects in Solar Flares. *Astrophys. J.* **2021**, *909*, 17. [[CrossRef](#)]
78. Malandraki, O.E.; Crosby, N.B. Solar Energetic Particles and Space Weather: Science and Applications. In *Solar Particle Radiation Storms Forecasting and Analysis*; Malandraki, O.E., Crosby, N.B., Eds.; Astrophysics and Space Science Library; Springer: Cham, Switzerland, 2018; Volume 444, pp. 1–26. [[CrossRef](#)]
79. McComas, D.J.; Christian, E.R.; Cohen, C.M.S.; Cummings, A.C.; Davis, A.J.; Desai, M.I.; Giacalone, J.; Hill, M.E.; Joyce, C.J.; Krimigis, S.M.; et al. Probing the energetic particle environment near the Sun. *Nature* **2019**, *576*, 223–227. [[CrossRef](#)] [[PubMed](#)]
80. Gómez-Herrero, R.; Pacheco, D.; Kollhoff, A.; Espinosa Lara, F.; Freiherr von Forstner, J.L.; Dresing, N.; Lario, D.; Balmaceda, L.; Krupar, V.; Malandraki, O.E.; et al. First near-relativistic solar electron events observed by EPD onboard Solar Orbiter. *Astron. Astrophys.* **2021**, *656*, L3. [[CrossRef](#)]
81. Pick, M.; Vilmer, N. Sixty-five years of solar radioastronomy: Flares, coronal mass ejections and Sun Earth connection. *Astron. Astrophys. Rev.* **2008**, *16*, 1–153. [[CrossRef](#)]
82. Reid, H.A.S.; Ratcliffe, H. A review of solar type III radio bursts. *Res. Astron. Astrophys.* **2014**, *14*, 773–804. [[CrossRef](#)]
83. Masson, S.; Antiochos, S.K.; DeVore, C.R. Escape of Flare-accelerated Particles in Solar Eruptive Events. *Astrophys. J.* **2019**, *884*, 143. [[CrossRef](#)]
84. Reid, H.A.S. A review of recent type III imaging spectroscopy. *Front. Astron. Space Sci.* **2020**, *7*, 56. [[CrossRef](#)]
85. Steinberg, J.L.; Aubier-Giraud, M.; Leblanc, Y.; Boisshot, A. Coronal Scattering, Absorption and Refraction of Solar Radiobursts. *Astron. Astrophys.* **1971**, *10*, 362.
86. Kontar, E.P.; Chen, X.; Chrysaphi, N.; Jeffrey, N.L.S.; Emslie, A.G.; Krupar, V.; Maksimovic, M.; Gordovskyy, M.; Browning, P.K. Anisotropic Radio-wave Scattering and the Interpretation of Solar Radio Emission Observations. *Astrophys. J.* **2019**, *884*, 122. [[CrossRef](#)]
87. Saint-Hilaire, P.; Krucker, S.; Christe, S.; Lin, R.P. The X-ray Detectability of Electron Beams Escaping from the Sun. *Astrophys. J.* **2009**, *696*, 941–952. [[CrossRef](#)]
88. Longcope, D.W.; Guidoni, S.E.; Linton, M.G. Gas-dynamic Shock Heating of Post-flare Loops Due to Retraction Following Localized, Impulsive Reconnection. *Astrophys. J. Lett.* **2009**, *690*, L18–L22. [[CrossRef](#)]
89. Reeves, K.K.; McCauley, P.L.; Tian, H. Direct Observations of Magnetic Reconnection Outflow and CME Triggering in a Small Erupting Solar Prominence. *Astrophys. J.* **2015**, *807*, 7. [[CrossRef](#)]
90. Zharkova, V.V.; Arzner, K.; Benz, A.O.; Browning, P.; Dauphin, C.; Emslie, A.G.; Fletcher, L.; Kontar, E.P.; Mann, G.; Onofri, M.; et al. Recent Advances in Understanding Particle Acceleration Processes in Solar Flares. *Space Sci. Rev.* **2011**, *159*, 357–420. [[CrossRef](#)]
91. Moore, R.L.; Sterling, A.C.; Hudson, H.S.; Lemen, J.R. Onset of the Magnetic Explosion in Solar Flares and Coronal Mass Ejections. *Astrophys. J.* **2001**, *552*, 833–848. [[CrossRef](#)]
92. Lin, J.; Forbes, T.G. Effects of reconnection on the coronal mass ejection process. *J. Geophys. Res.* **2000**, *105*, 2375–2392. [[CrossRef](#)]
93. Antiochos, S.K.; DeVore, C.R.; Klimchuk, J.A. A Model for Solar Coronal Mass Ejections. *Astrophys. J.* **1999**, *510*, 485–493. [[CrossRef](#)]
94. Török, T.; Kliem, B. Confined and Ejective Eruptions of Kink-unstable Flux Ropes. *Astrophys. J. Lett.* **2005**, *630*, L97–L100. [[CrossRef](#)]
95. Wyper, P.F.; DeVore, C.R.; Antiochos, S.K. A Breakout Model for Solar Coronal Jets with Filaments. *Astrophys. J.* **2018**, *852*, 98. [[CrossRef](#)]
96. Pariat, E.; Dalmasse, K.; DeVore, C.R.; Antiochos, S.K.; Karpen, J.T. A model for straight and helical solar jets. II. Parametric study of the plasma beta. *Astron. Astrophys.* **2016**, *596*, A36. [[CrossRef](#)] [[PubMed](#)]
97. Pariat, E.; Dalmasse, K.; DeVore, C.R.; Antiochos, S.K.; Karpen, J.T. Model for straight and helical solar jets. I. Parametric studies of the magnetic field geometry. *Astron. Astrophys.* **2015**, *573*, A130. [[CrossRef](#)]
98. Wyper, P.F.; DeVore, C.R.; Karpen, J.T.; Antiochos, S.K.; Yeates, A.R. A Model for Coronal Hole Bright Points and Jets Due to Moving Magnetic Elements. *Astrophys. J.* **2018**, *864*, 165. [[CrossRef](#)]
99. Parnell, C.E.; De Moortel, I. A contemporary view of coronal heating. *Philos. Trans. R. Soc. Lond. Ser. A* **2012**, *370*, 3217–3240. [[CrossRef](#)]
100. Klimchuk, J.A. On Solving the Coronal Heating Problem. *Sol. Phys.* **2006**, *234*, 41–77. [[CrossRef](#)]
101. Klimchuk, J.A. Key aspects of coronal heating. *Philos. Trans. R. Soc. Lond. Ser. A* **2015**, *373*, 20140256. [[CrossRef](#)] [[PubMed](#)]
102. Klimchuk, J.A.; Luna, M. The Role of Asymmetries in Thermal Nonequilibrium. *Astrophys. J.* **2019**, *884*, 68. [[CrossRef](#)]
103. Viall, N.M.; Borovsky, J.E. Nine Outstanding Questions of Solar Wind Physics. *J. Geophys. Res. (Space Phys.)* **2020**, *125*, e26005. [[CrossRef](#)] [[PubMed](#)]
104. Hannah, I.G.; Hudson, H.S.; Battaglia, M.; Christe, S.; Kašparová, J.; Krucker, S.; Kundu, M.R.; Veronig, A. Microflares and the Statistics of X-ray Flares. *Space Sci. Rev.* **2011**, *159*, 263–300. [[CrossRef](#)]
105. Testa, P.; De Pontieu, B.; Allred, J.; Carlsson, M.; Reale, F.; Daw, A.; Hansteen, V.; Martinez-Sykora, J.; Liu, W.; DeLuca, E.E.; et al. Evidence of nonthermal particles in coronal loops heated impulsively by nanoflares. *Science* **2014**, *346*, 1255724. [[CrossRef](#)] [[PubMed](#)]
106. Dudík, J.; Dzifčáková, E.; Meyer-Vernet, N.; Del Zanna, G.; Young, P.R.; Giunta, A.; Sylwester, B.; Sylwester, J.; Oka, M.; Mason, H.E.; et al. Nonequilibrium Processes in the Solar Corona, Transition Region, Flares, and Solar Wind (Invited Review). *Sol. Phys.* **2017**, *292*, 100. [[CrossRef](#)]

107. Benz, A.O.; Grigis, P.C. Microflares and hot component in solar active regions. *Sol. Phys.* **2002**, *210*, 431–444. [[CrossRef](#)]
108. Krucker, S.; Christe, S.; Lin, R.P.; Hurford, G.J.; Schwartz, R.A. Hard X-ray Microflares down to 3 keV. *Sol. Phys.* **2002**, *210*, 445–456. [[CrossRef](#)]
109. Christe, S.; Hannah, I.G.; Krucker, S.; McTiernan, J.; Lin, R.P. RHESSI Microflare Statistics. I. Flare-Finding and Frequency Distributions. *Astrophys. J.* **2008**, *677*, 1385–1394. [[CrossRef](#)]
110. Warmuth, A.; Mann, G. Constraints on energy release in solar flares from RHESSI and GOES X-ray observations. II. Energetics and energy partition. *Astron. Astrophys.* **2016**, *588*, A116. [[CrossRef](#)]
111. Hannah, I.G.; Christe, S.; Krucker, S.; Hurford, G.J.; Hudson, H.S.; Lin, R.P. RHESSI Microflare Statistics. II. X-Ray Imaging, Spectroscopy, and Energy Distributions. *Astrophys. J.* **2008**, *677*, 704–718. [[CrossRef](#)]
112. Battaglia, A.F.; Saqri, J.; Massa, P.; Perracchione, E.; Dickson, E.C.M.; Xiao, H.; Veronig, A.M.; Warmuth, A.; Battaglia, M.; Hurford, G.J.; et al. STIX X-ray microflare observations during the Solar Orbiter commissioning phase. *Astron. Astrophys.* **2021**, *656*, A4. [[CrossRef](#)]
113. Saqri, J.; Veronig, A.M.; Warmuth, A.; Dickson, E.C.M.; Battaglia, A.F.; Podladchikova, T.; Xiao, H.; Battaglia, M.; Hurford, G.J.; Krucker, S. Multi-instrument STIX microflare study. *Astron. Astrophys.* **2022**, *659*, A52. [[CrossRef](#)]
114. Glesener, L.; Krucker, S.; Duncan, J.; Hannah, I.G.; Grefenstette, B.W.; Chen, B.; Smith, D.M.; White, S.M.; Hudson, H. Accelerated Electrons Observed Down to <7 keV in a NuSTAR Solar Microflare. *Astrophys. J. Lett.* **2020**, *891*, L34. [[CrossRef](#)] [[PubMed](#)]
115. Cooper, K.; Hannah, I.G.; Grefenstette, B.W.; Glesener, L.; Krucker, S.; Hudson, H.S.; White, S.M.; Smith, D.M.; Duncan, J. NuSTAR observations of a repeatedly microflaring active region. *Mon. Not. RAS* **2021**, *507*, 3936–3951. [[CrossRef](#)] [[PubMed](#)]
116. Duncan, J.; Glesener, L.; Grefenstette, B.W.; Vievering, J.; Hannah, I.G.; Smith, D.M.; Krucker, S.; White, S.M.; Hudson, H. NuSTAR Observation of Energy Release in 11 Solar Microflares. *Astrophys. J.* **2021**, *908*, 29. [[CrossRef](#)] [[PubMed](#)]
117. Polito, V.; Peterson, M.; Glesener, L.; Testa, P.; Yu, S.; Reeves, K.K.; Sun, X.; Duncan, J. Multi-wavelength observations and modeling of a microflare: Constraining non-thermal particle acceleration. *Front. Astron. Space Sci.* **2023**, *10*, 1214901. [[CrossRef](#)]
118. Warmuth, A.; Mann, G. Thermal-nonthermal energy partition in solar flares derived from X-ray, EUV, and bolometric observations. Discussion of recent studies. *Astron. Astrophys.* **2020**, *644*, A172. [[CrossRef](#)]
119. Schmelz, J.T.; Kashyap, V.L.; Saar, S.H.; Dennis, B.R.; Grigis, P.C.; Lin, L.; De Luca, E.E.; Holman, G.D.; Golub, L.; Weber, M.A. Some Like It Hot: Coronal Heating Observations from Hinode X-ray Telescope and RHESSI. *Astrophys. J.* **2009**, *704*, 863–869. [[CrossRef](#)]
120. Brosius, J.W.; Daw, A.N.; Rabin, D.M. Pervasive Faint Fe XIX Emission from a Solar Active Region Observed with EUNIS-13: Evidence for Nanoflare Heating. *Astrophys. J.* **2014**, *790*, 112. [[CrossRef](#)]
121. Caspi, A.; Woods, T.N.; Warren, H.P. New Observations of the Solar 0.5–5 keV Soft X-Ray Spectrum. *Astrophys. J. Lett.* **2015**, *802*, L2. [[CrossRef](#)]
122. Del Zanna, G.; Andretta, V.; Cargill, P.J.; Corso, A.J.; Daw, A.N.; Golub, L.; Klimchuk, J.A.; Mason, H.E. High resolution soft X-ray spectroscopy and the quest for the hot (5–10 MK) plasma in solar active regions. *Front. Astron. Space Sci.* **2021**, *8*, 33. [[CrossRef](#)]
123. Bradshaw, S.J.; Klimchuk, J.A. What Dominates the Coronal Emission Spectrum During the Cycle of Impulsive Heating and Cooling? *Astrophys. J. Suppl.* **2011**, *194*, 26. [[CrossRef](#)]
124. Golub, L.; Hartquist, T.W.; Quillen, A.C. Comments on the Observability of Coronal Variations. *Sol. Phys.* **1989**, *122*, 245–261. [[CrossRef](#)]
125. Reale, F.; Orlando, S. Nonequilibrium of Ionization and the Detection of Hot Plasma in Nanoflare-heated Coronal Loops. *Astrophys. J.* **2008**, *684*, 715–724. [[CrossRef](#)]
126. Lörinčík, J.; Dudík, J.; del Zanna, G.; Džifčáková, E.; Mason, H.E. Plasma Diagnostics from Active Region and Quiet-Sun Spectra Observed by Hinode/EIS: Quantifying the Departures from a Maxwellian Distribution. *Astrophys. J.* **2020**, *893*, 34. [[CrossRef](#)]
127. Džifčáková, E.; Dudík, J.; Zemanová, A.; Lörinčík, J.; Karlický, M. KAPPA: A Package for the Synthesis of Optically Thin Spectra for the Non-Maxwellian  $\kappa$ -distributions. II. Major Update to Compatibility with CHIANTI Version 10. *Astrophys. J. Suppl.* **2021**, *257*, 62. [[CrossRef](#)]
128. Del Zanna, G.; Polito, V.; Dudík, J.; Testa, P.; Mason, H.E.; Džifčáková, E. Diagnostics of Non-Maxwellian Electron Distributions in Solar Active Regions from Fe XII Lines Observed by the Hinode Extreme Ultraviolet Imaging Spectrometer and Interface Region Imaging Spectrograph. *Astrophys. J.* **2022**, *930*, 61. [[CrossRef](#)]
129. Ishikawa, S.n.; Glesener, L.; Krucker, S.; Christe, S.; Buitrago-Casas, J.C.; Narukage, N.; Vievering, J. Detection of nanoflare-heated plasma in the solar corona by the FOXSI-2 sounding rocket. *Nat. Astron.* **2017**, *1*, 771–774. [[CrossRef](#)]
130. Moore, C.S.; Caspi, A.; Woods, T.N.; Chamberlin, P.C.; Dennis, B.R.; Jones, A.R.; Mason, J.P.; Schwartz, R.A.; Tolbert, A.K. The Instruments and Capabilities of the Miniature X-Ray Solar Spectrometer (MinXSS) CubeSats. *Sol. Phys.* **2018**, *293*, 21. [[CrossRef](#)]
131. Marsh, A.J.; Smith, D.M.; Glesener, L.; Klimchuk, J.A.; Bradshaw, S.J.; Vievering, J.; Hannah, I.G.; Christe, S.; Ishikawa, S.n.; Krucker, S. Hard X-Ray Constraints on Small-scale Coronal Heating Events. *Astrophys. J.* **2018**, *864*, 5. [[CrossRef](#)]
132. Mandrini, C.H.; Démoulin, P.; Klimchuk, J.A. Magnetic Field and Plasma Scaling Laws: Their Implications for Coronal Heating Models. *Astrophys. J.* **2000**, *530*, 999–1015. [[CrossRef](#)]
133. Cranmer, S.R.; Winebarger, A.R. The Properties of the Solar Corona and Its Connection to the Solar Wind. *Annu. Rev. Astron. Astrophys.* **2019**, *57*, 157–187. [[CrossRef](#)]
134. Brooks, D.H.; Warren, H.P.; Landi, E. Measurements of Coronal Magnetic Field Strengths in Solar Active Region Loops. *Astrophys. J. Lett.* **2021**, *915*, L24. [[CrossRef](#)]

135. Hurford, G.J. X-ray imaging with collimators, masks and grids. *Issi Sci. Rep. Ser.* **2010**, *9*, 223–234.
136. Piana, M.; Emslie, A.; Massone, A.M.; Dennis, B.R. *Hard X-ray Imaging of Solar Flares*; Springer: Berlin/Heidelberg, Germany, 2022.
137. Massa, P.; Hurford, G.J.; Volpara, A.; Kuhar, M.; Battaglia, A.F.; Xiao, H.; Casadei, D.; Perracchione, E.; Garbarino, S.; Guastavino, S.; et al. STIX imaging I—Concept. *arXiv* **2023**, arXiv:2303.02485. [[CrossRef](#)]
138. Christe, S.; Alaoui, M.; Allred, J.; Battaglia, M.; Baumgartner, W.; Buitrago-Casas, J.C.; Chen, B.; Chen, T.; Dennis, B.; Drake, J.; et al. The Focusing Optics X-ray Solar Imager (FOXSI). *Bull. Am. Astron. Soc.* **2023**, *55*, 065. [[CrossRef](#)]
139. Krucker, S.; Christe, S.; Glesener, L.; Ishikawa, S.n.; Ramsey, B.; Takahashi, T.; Watanabe, S.; Saito, S.; Gubarev, M.; Kilaru, K.; et al. First Images from the Focusing Optics X-Ray Solar Imager. *Astrophys. J. Lett.* **2014**, *793*, L32. [[CrossRef](#)]
140. Christe, S.; Glesener, L.; Buitrago-Casas, C.; Ishikawa, S.N.; Ramsey, B.; Gubarev, M.; Kilaru, K.; Kolodziejczak, J.J.; Watanabe, S.; Takahashi, T.; et al. FOXSI-2: Upgrades of the Focusing Optics X-ray Solar Imager for its Second Flight. *J. Astron. Instrum.* **2016**, *5*, 1640005–1640625. [[CrossRef](#)]
141. Glesener, L.; Krucker, S.; Christe, S.; Ishikawa, S.n.; Buitrago-Casas, J.C.; Ramsey, B.; Gubarev, M.; Takahashi, T.; Watanabe, S.; Takeda, S.; et al. The FOXSI solar sounding rocket campaigns. In *Space Telescopes and Instrumentation 2016: Ultraviolet to Gamma Ray*; den Herder, J.W.A., Takahashi, T., Bautz, M., Eds.; Society of Photo-Optical Instrumentation Engineers (SPIE) Conference Series; SPIE: Bellingham, WA, USA, 2016; Volume 9905, p. 99050E. [[CrossRef](#)]
142. Musset, S.; Buitrago-Casas, J.C.; Glesener, L.; Bongiorno, S.; Courtade, S.; Athiray, P.S.; Vievering, J.; Ishikawa, S.n.; Narukage, N.; Furukawa, K.; et al. Ghost-ray reduction and early results from the third FOXSI sounding rocket flight. In *UV, X-ray, and Gamma-Ray Space Instrumentation for Astronomy XXI*; Society of Photo-Optical Instrumentation Engineers (SPIE) Conference Series; SPIE: Bellingham, WA, USA, 2019; Volume 11118, p. 1111812. [[CrossRef](#)]
143. Christe, S.D.; Shih, A.; Rodriguez, M.; Cramer, A.; Gregory, K.; Edgerton, M.; Gaskin, J.; Wilson-Hodge, C.; Apple, J.; Stevenson Chavis, K.; et al. The high energy replicated optics to explore the sun mission: A hard x-ray balloon-borne telescope. In *Solar Physics and Space Weather Instrumentation V*; Fineschi, S., Fennelly, J., Eds.; Society of Photo-Optical Instrumentation Engineers (SPIE) Conference Series; SPIE: Bellingham, WA, USA, 2013; Volume 8862, p. 886206. [[CrossRef](#)]
144. Christe, S.; Shih, A.Y.; Rodriguez, M.; Cramer, A.; Gregory, K.; Gaskin, J.; Chavis, K.; Smith, L.; HOPE/HEROES Team. The High Energy Replicated Optics to Explore the Sun (HEROES). In Proceedings of the AAS/Solar Physics Division Abstracts #44, July 2013; AAS/Solar Physics Division Meeting; Volume 44, p. 100.76.
145. Allington-Smith, J. Basic principles of integral field spectroscopy. *New Astron. Rev.* **2006**, *50*, 244–251. [[CrossRef](#)]
146. Del Zanna, G.; Mason, H.E. Solar UV and X-ray spectral diagnostics. *Living Rev. Sol. Phys.* **2018**, *15*, 5. [[CrossRef](#)] [[PubMed](#)]
147. Landi, E.; Hutton, R.; Brage, T.; Li, W. Hinode/EIS Measurements of Active-region Magnetic Fields. *Astrophys. J.* **2020**, *904*, 87. [[CrossRef](#)]
148. Dudík, J.; Del Zanna, G.; Mason, H.E.; Dzifčáková, E. Signatures of the non-Maxwellian  $\kappa$ -distributions in optically thin line spectra. I. Theory and synthetic Fe IX–XIII spectra. *Astron. Astrophys.* **2014**, *570*, A124. [[CrossRef](#)]
149. Dudík, J.; Mackovjak, Š.; Dzifčáková, E.; Del Zanna, G.; Williams, D.R.; Karlický, M.; Mason, H.E.; Lörinčík, J.; Kotrč, P.; Fárník, F.; et al. Imaging and Spectroscopic Observations of a Transient Coronal Loop: Evidence for the Non-Maxwellian  $\kappa$  Distributions. *Astrophys. J.* **2015**, *807*, 123. [[CrossRef](#)]
150. Matthews, S.A.; Reid, H.A.S.; Baker, D.; Bloomfield, D.S.; Browning, P.K.; Calcines, A.; Del Zanna, G.; Erdelyi, R.; Fletcher, L.; Hannah, I.G.; et al. The high-energy Sun—probing the origins of particle acceleration on our nearest star. *Exp. Astron.* **2022**, *54*, 335–360. [[CrossRef](#)]

**Disclaimer/Publisher’s Note:** The statements, opinions and data contained in all publications are solely those of the individual author(s) and contributor(s) and not of MDPI and/or the editor(s). MDPI and/or the editor(s) disclaim responsibility for any injury to people or property resulting from any ideas, methods, instructions or products referred to in the content.